

Composite Superconducting Orders and Magnetism in CeRh_2As_2

Fabian Jakubczyk,^{*} Julia M. Link, and Carsten Timm[†]
*Institute of Theoretical Physics and Würzburg-Dresden Cluster of
 Excellence ct.qmat, Technische Universität Dresden, 01069 Dresden*
 (Dated: June 11, 2025)

Locally noncentrosymmetric materials are attracting significant attention due to the unique phenomena associated with sublattice degrees of freedom. The recently discovered heavy-fermion superconductor CeRh_2As_2 has emerged as a compelling example of this class, garnering widespread interest for its remarkable temperature-magnetic-field phase diagram, which features a field-induced first-order superconductor-to-superconductor phase transition with nontrivial dependence on the field direction and high critical fields, as well as antiferromagnetic and potentially higher multipole orders. To investigate the complex interplay of the ordered phases in CeRh_2As_2 , we develop a theoretical framework based on symmetry analysis combined with Bogoliubov–de Gennes and Landau methods. This approach allows us to propose probable symmetries of the superconducting states and elucidate their close relationship with magnetism. Intriguingly, we find that the first-order transition can be interpreted as a transition between coexistence phases of the same symmetry but with distinct admixtures of individual superconducting order parameters. This line may end in a critical endpoint below the superconducting critical temperature. Our approach accurately reproduces current experimental phase diagrams for varying temperature as well as out-of-plane and in-plane magnetic field, both if the transition to a magnetic phase occurs below the superconducting critical temperature and if it occurs above. Furthermore, we calculate the magnetic susceptibility and the specific heat and compare these quantities to recent experimental results.

I. INTRODUCTION

Layered materials that overall possess inversion symmetry while the separate layers do not have this symmetry show intriguing superconducting phenomena enabled by the sublattice degrees of freedom [1–4]. A particularly interesting example is the heavy-fermion material CeRh_2As_2 , which has recently received attention due to its remarkable multiphase superconductivity [5]. The material becomes superconducting at $T_c \approx 260$ mK based on the magnetic susceptibility (Meißner–Ochsenfeld effect) [5]. A magnetic field applied along the crystallographic c -axis suppresses T_c but the suppression is weaker than expected for Pauli limiting in a conventional superconductor [5]. A key feature is the field-induced first-order transition between different superconducting orders at about 4 T, which depends only weakly on temperature [5]. The high-field phase is only very weakly suppressed when the field is further increased and thus evidently avoids Pauli limiting [5], with an extrapolated upper critical field at zero temperature of about 14 T. The first-order transition is widely interpreted as an even-to-odd-parity transition, with a potential (pseudo-) spin-triplet high-field superconducting state [5–9].

On the other hand, a magnetic field applied in the ab plane suppresses the low-field superconducting phase at an upper critical field of 1.9 T, consistent with Pauli limiting [5]. No transition to another superconducting phase is observed for a magnetic field in plane. However, additional phase transitions are clearly seen in several ob-

servables at stronger field and higher temperatures [10]. A “phase I” completely surrounds the superconducting phase in the temperature-magnetic-field plane. Its critical temperature T_0 grows with increasing field strength within the plane [10, 11]. The phase gives way to a “phase II” at a first-order transition at a weakly temperature-dependent field of about 9 T and the critical temperature T_0 further increases with field [10, 11]. The phases I and II were suggested to exhibit quadrupolar order since they are not visible in the magnetic dipolar response and because the enhancement of T_0 with magnetic field is hard to understand for dipolar order [10, 12].

Beyond exhibiting multiple superconducting phases, CeRh_2As_2 also demonstrates the coexistence of magnetism and superconductivity. On the one hand, ^{75}As nuclear quadrupole resonance (NQR) [13] and nuclear magnetic resonance (NMR) [8, 14] exhibit an onset of magnetic order below the superconducting transition. On the other hand, recent muon spin relaxation (μSR) data [15] suggest that phase I, which sets in at $T_0 = 0.55$ K, above the superconducting critical temperature of $T_c = 0.3$ K, in fact involves magnetic dipolar order.

In this work, we study the interplay between competing orders in CeRh_2As_2 applying symmetry analysis and free-energy expansion in terms of multiple order parameters. This approach allows us to identify the symmetry of the dominant superconducting pairing states as well as the magnetic phase. We find that the low-field phase is dominated by even parity, spin-singlet B_{1g+} pairing, whereas the high-field phase shows a predominant odd-parity, spin-triplet B_{1u+} contribution. The magnetic order parameter (OP) likely has A_{1u-} symmetry and is antiferromagnetic (AFM). However, the situation is more complex since we find an admixture of all three OPs in various regions of realistic phase dia-

^{*} fabian.jakubczyk@tu-dresden.de

[†] carsten.timm@tu-dresden.de

grams. This is accompanied by the novel observation of a symmetry-preserving first-order transition between coexistence phases of the same overall symmetry, yet with distinct proportions of the individual superconducting OPs. Moreover, the symmetry-preserving first-order transition allows and we indeed predict that the first-order line ends in a critical endpoint. Beyond this point, the low-field and high-field phases are connected by a crossover region. Our approach coherently reproduces state-of-the-art experimental results for both orderings of the superconducting critical temperature T_c and the Néel temperature of the magnetic order, $T_N > T_c$ and $T_N < T_c$, while introducing the important perspective of not just multiphase, but also multicomponent superconductivity in CeRh_2As_2 . These multicomponent phases involve non-degenerate composite OPs of distinct irreducible representations and amplitudes, as opposed to the case of OPs that belong to the same irreducible representation and are degenerate by symmetry.

The remainder of this paper is structured as follows. In Sec. II, we introduce our symmetry-informed model for the normal state of CeRh_2As_2 . In Sec. III, we then analyze which superconducting pairing states might exist and which are most likely in the absence of an applied magnetic field. Section IV discusses the magnetic order observed in CeRh_2As_2 and its coexistence with superconductivity. In Sec. V, we investigate the effect of a magnetic field on the superconducting order, depending on the field direction. Section VI first introduces the Landau free-energy expansion for our model and then presents our main results for phase diagrams in the temperature-magnetic-field plane for various magnetic-field directions and both cases $T_N > T_c$ and $T_N < T_c$. We also show plots of the OPs and the free energy vs. magnetic field or temperature for cuts through the phase diagrams and discuss their interpretation. In Sec. VII, we briefly discuss thermodynamic signatures visible in the susceptibility and specific heat for $T_N > T_c$ and a field out of plane. We summarize our work and draw conclusions in Sec. VIII.

II. MODEL AND NORMAL STATE

CeRh_2As_2 is a layered compound with CaBe_2Ge_2 -type crystal structure, nonsymmorphic space group $P4/nmm$ and point group is D_{4h} . The structure contains square lattices of Ce atoms and alternating inequivalent spacer layers, as shown in Fig. 1. The unit cell contains two Ce atoms in adjacent layers. The inversion centers are located between the Ce layers, whereas there are no inversion centers within the layers.

We use an effective model with a single doublet per Ce atom, resulting in a 4×4 normal-state Hamiltonian. The Hamiltonian can be expanded into Kronecker products of Pauli and identity matrices, $\tau_i \otimes \sigma_j$, where the first factor acts on the basis site (sublattice) and the second on spin. The ground states likely form a Γ_7 ($E_{3/2}$) doublet of the local point group C_{4v} at the Ce site [10]. The first ex-

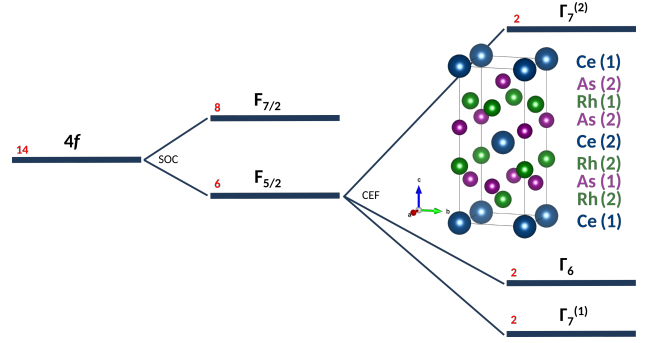


FIG. 1. Schematic of the CeRh_2As_2 level splitting with the inset showing the crystal structure with distinct lattice planes. The f -orbital degeneracy is lifted by strong spin-orbit coupling and the $J = 5/2$ multiplet of Ce^{3+} is split by the crystal electric field into three Kramers doublets [5, 10].

cited doublet of Γ_6 ($E_{1/2}$) symmetry is about 30 K above the ground-state doublet. Since $E_{3/2} = E_{1/2} \otimes B_1$ the ground-state doublet transforms differently from a spin, i.e., from a $E_{1/2}$ doublet, and we assume $E_{3/2}$ when writing down the representations of symmetry operations. However, the additional signs compared to $E_{1/2}$ drop out for bilinear forms and therefore do not affect the results. For simplicity, we refer to the $E_{3/2}$ degree of freedom as a “spin.” The energy splitting and the crystal structure are shown in Fig. 1.

Spatial inversion is described by

$$P = \tau_x \otimes \sigma_0 \quad (1)$$

since inversion interchanges the two Ce sites but leaves the spin invariant. Fourfold rotation about the z -axis and twofold rotations about the x -axis are described by

$$C_{4z} = -\tau_0 \otimes e^{-i\pi\sigma_z/4}, \quad (2)$$

$$C_{2x} = \tau_x \otimes e^{-i\pi\sigma_x/2}, \quad (3)$$

respectively. These representations imply that the twofold rotation about the $[110]$ direction is described by

$$C_{2xy} = \tau_x \otimes e^{-i\pi(\sigma_x + \sigma_y)/2\sqrt{2}}. \quad (4)$$

Finally, the unitary part of the antiunitary time-reversal (TR) operator is

$$U_T = \tau_0 \otimes i\sigma_y. \quad (5)$$

The matrices in sublattice and spin space are irreducible tensor operators of irreps of the gray group D_{4h} . The basis matrices and their irreps inferred from Eqs. (1)–(5) are given in Table I. We are using real, i.e., orthogonal, irreps and the sign “ \pm ” in the subscript refers to the behavior under TR [16]. The irreps of the 4×4 basis matrices then follow from the usual rules for products of representations and are shown in Table II.

TABLE I. Irreps of basis matrices acting on basis-site (sublattice) space, τ_i , and on spin space, σ_j . For the components of the E_{g-} doublet, we take the standard convention: The first element is invariant under C_{2x} and is transformed into the second by C_{4z} .

| | |
|--|-----------|
| τ_0 | A_{1g+} |
| τ_x | A_{1g+} |
| τ_y | A_{2u-} |
| τ_z | A_{2u+} |
| σ_0 | A_{1g+} |
| $\begin{pmatrix} \sigma_x \\ \sigma_y \end{pmatrix}$ | E_{g-} |
| σ_z | A_{2g-} |

The normal-state Hamiltonian $H_N(\mathbf{k})$ can be expanded into these basis matrices with momentum-dependent form factors as

$$H_N(\mathbf{k}) = \sum_n c_n(\mathbf{k}) h_n, \quad (6)$$

where the combination must be invariant under the point group, i.e., must belong to the trivial irrep A_{1g+} . Table III shows the possible TR-even products of irreps for the basis matrices and the form factors, as well as the minimum order l of polynomial form factors. As noted, in $H_N(\mathbf{k})$ only combinations belonging to A_{1g+} can occur, they are highlighted by bold face. The corresponding basis matrices can be read off from Table II:

$$h_0 = \tau_0 \otimes \sigma_0 \quad A_{1g+}, \quad (7)$$

$$h_1 = \tau_x \otimes \sigma_0 \quad A_{1g+}, \quad (8)$$

TABLE II. Irreps of 4×4 ($\tau_i \otimes \sigma_j$) basis matrices on combined sublattice-spin space for our model for CeRh₂As₂.

| | |
|---|-----------|
| $\tau_0 \otimes \sigma_0$ | A_{1g+} |
| $\begin{pmatrix} \tau_0 \otimes \sigma_x \\ \tau_0 \otimes \sigma_y \end{pmatrix}$ | E_{g-} |
| $\tau_0 \otimes \sigma_z$ | A_{2g-} |
| $\tau_x \otimes \sigma_0$ | A_{1g+} |
| $\begin{pmatrix} \tau_x \otimes \sigma_x \\ \tau_x \otimes \sigma_y \end{pmatrix}$ | E_{g-} |
| $\tau_x \otimes \sigma_z$ | A_{2g-} |
| $\tau_y \otimes \sigma_0$ | A_{2u-} |
| $\begin{pmatrix} \tau_y \otimes \sigma_y \\ -\tau_y \otimes \sigma_x \end{pmatrix}$ | E_{u+} |
| $\tau_y \otimes \sigma_z$ | A_{1u+} |
| $\tau_z \otimes \sigma_0$ | A_{2u+} |
| $\begin{pmatrix} \tau_z \otimes \sigma_y \\ -\tau_z \otimes \sigma_x \end{pmatrix}$ | E_{u-} |
| $\tau_z \otimes \sigma_z$ | A_{1u-} |

$$h_2 = \tau_y \otimes \sigma_0 \quad A_{2u-}, \quad (9)$$

$$h_3 = \tau_z \otimes \sigma_y \quad E_{u-}, \quad (10)$$

$$h_4 = -\tau_z \otimes \sigma_x \quad E_{u-}, \quad (11)$$

$$h_5 = \tau_z \otimes \sigma_z \quad A_{1u-}. \quad (12)$$

These matrices are also used by Amin *et al.* [17]. They satisfy the standard algebra of gamma matrices for inversion-symmetric models with four-valued internal degrees of freedom [16]: h_1, \dots, h_5 anticommute with each other and h_0 commutes with all of them. The dispersion in the normal state is thus

$$\xi(\mathbf{k}) = c_0(\mathbf{k}) \pm \sqrt{c_1^2(\mathbf{k}) + \dots + c_5^2(\mathbf{k})}, \quad (13)$$

where each band is twofold degenerate. Since $c_1(\mathbf{k})$ belongs to A_{1g+} it generically contains a \mathbf{k} -independent term so that the root is nonzero even at $\mathbf{k} = 0$. Hence, we do not expect band-touching points in the normal state.

III. SUPERCONDUCTING PARING STATES

In order to understand the unconventional phase diagram of CeRh₂As₂, we have to consider properties of the material that go beyond generic materials with D_{4h} point group: (1) The material consists of relatively weakly coupled layers, (2) the inversion centers lie between these layers, and (3) the Ce f -electrons carry a relatively large spectral weight close to the Fermi energy. The layered nature of the material suggests that the strongest (pairing) interactions are in plane. This observation together with the fact that the inversion centers are between the layers implies that any two pairing states that are only distinguished by their symmetry under inversion are close in energy [5, 7]. Cavanagh *et al.* [7] find that the nonsymmorphic space group together with large density of states at the Fermi energy resulting from bands close to the Brillouin-zone boundaries also lead to near-degeneracy of such pairing states.

The superconducting states are described by the 8×8 Bogoliubov–de Gennes (BdG) Hamiltonian

$$\mathcal{H}(\mathbf{k}) = \begin{pmatrix} H_N(\mathbf{k}) & \Delta(\mathbf{k}) \\ \Delta^\dagger(\mathbf{k}) & -H_N^T(-\mathbf{k}) \end{pmatrix}. \quad (14)$$

The basis matrices h_n for the normal state are lifted to BdG–Nambu space according to

$$h_n \mapsto \begin{pmatrix} h_n & 0 \\ 0 & -P^* h_n^T P^T \end{pmatrix}. \quad (15)$$

It is useful to write the pairing matrix as

$$\Delta(\mathbf{k}) = D(\mathbf{k}) U_T, \quad (16)$$

where $D(\mathbf{k})$, unlike $\Delta(\mathbf{k})$, transforms like a matrix under point-group transformations [16], which facilitates

TABLE III. Time-reversal-even products of irreps of basis matrices and form factors. l denotes the angular momentum of the form factors, i.e., the lowest possible order of a polynomial basis function of the respective irrep. Here, $X_{u+} = A_{1u+} \oplus A_{2u+} \oplus B_{1u+} \oplus B_{2u+}$ and $X_{g+} = A_{1g+} \oplus A_{2g+} \oplus B_{1g+} \oplus B_{2g+}$. Combinations invariant under the point group are highlighted by bold face.

| form factor | l | A_{1g+} | A_{2g-} | E_{g-} | A_{1u+} | A_{1u-} | A_{2u+} | A_{2u-} | E_{u+} | E_{u-} |
|-------------|-----|-----------------------------|-----------|----------|-----------|-----------------------------|-----------|-----------------------------|----------|----------------------------|
| A_{1g+} | 0 | A_{1g+} | | | A_{1u+} | | A_{2u+} | | E_{u+} | |
| A_{2g+} | 4 | A_{2g+} | | | A_{2u+} | | A_{1u+} | | E_{u+} | |
| B_{1g+} | 2 | B_{1g+} | | | B_{1u+} | | B_{2u+} | | E_{u+} | |
| B_{2g+} | 2 | B_{2g+} | | | B_{2u+} | | B_{1u+} | | E_{u+} | |
| E_{g+} | 2 | E_{g+} | | | E_{u+} | | E_{u+} | | X_{u+} | |
| A_{1u-} | 5 | | A_{2u+} | E_{u+} | | A_{1g+} | | A_{2g+} | | E_{g+} |
| A_{2u-} | 1 | | A_{1u+} | E_{u+} | | A_{2g+} | | A_{1g+} | | E_{g+} |
| B_{1u-} | 3 | | B_{2u+} | E_{u+} | | B_{1g+} | | B_{2g+} | | E_{g+} |
| B_{2u-} | 3 | | B_{1u+} | E_{u+} | | B_{2g+} | | B_{1g+} | | E_{g+} |
| E_{u-} | 1 | | E_{u+} | X_{u+} | | E_{g+} | | E_{g+} | | X_{g+} |

the symmetry analysis. $D(\mathbf{k})$ can be expanded into basis matrices from Table II with momentum-dependent form factors. Unlike the normal-state block $H_N(\mathbf{k})$, $D(\mathbf{k})$ need not transform trivially (A_{1g+}) under the point group since the superconducting state can break the lattice symmetry spontaneously. However, contributions that are odd under TR cannot occur since only TR-even irreps (subscript “+”) are compatible with fermionic anti-symmetry [16].

The specific-heat jump at the superconducting transition suggests a strongly enhanced effective mass, which implies that CeRh₂As₂ is a heavy-fermion material with significant Ce f -orbital weight at the Fermi energy [7]. Standard DFT is unable to describe this mass enhancement but including renormalization of the bands due to strong correlations [18, 19] provides a band structure with rather flat bands with large f -orbital weight at the Fermi energy [7]. However, Nogaki *et al.* [20] obtained rather flat f bands without this renormalization. The flat bands imply that the Fermi surface is very sensitive to small changes in parameters such as the chemical potential, both theoretically and experimentally. Because of the large f -electron weight the onsite Hubbard repulsion U is expected to be strong. Therefore, we do not expect an on-site attractive pairing interaction to exist. On the contrary, any pairing state that has a contribution from on-site pairing is expected to be disfavored by the Hubbard repulsion. This applies to pairing matrices $\Delta(\mathbf{k}) = D(\mathbf{k})U_T$ which satisfy three conditions: (a) $D(\mathbf{k})$ describes pairing at the same basis site, i.e., it contains τ_0 or τ_z . (b) $D(\mathbf{k})$ describes spin-singlet pairing, i.e., it contains σ_0 , because our model has only a single orbital per Ce site and local spin-triplet pairing is excluded by the Pauli principle. (c) The form factor contains a momentum-independent (local) term and thus necessarily has A_{1g+} symmetry.

The basis matrices resulting from (a) and (b) are $\tau_0 \otimes \sigma_0$ (A_{1g+}) and $\tau_z \otimes \sigma_0$ (A_{2u+}). Both are compatible with a A_{1g+} form factor so that condition (c) does not lead to a

further reduction. We conclude that pairing states with A_{1g+} and A_{2u+} symmetry are disfavored by the Hubbard U .

So far, we have argued that the strongest interactions are likely in plane but are repulsive on site. Due to the localization of f -orbitals and the relatively strong screening due to a high density of states at the Fermi energy, we do not expect strong longer-range repulsive Coulomb interactions. Hence, it is natural to assume that the dominant pairing interaction is in plane, of short range, but not local. In the absence of arguments to the contrary, the leading contribution to superconductivity is assumed to be in-plane nearest-neighbor pairing. Which pairing matrices are compatible with this? First, they must contain τ_0 or τ_z because τ_x and τ_y describe interlayer pairing. These correspond to the first and last block in Table II, including irreps of A_{1g+} , A_{2g-} , E_{g-} , A_{1u-} , A_{2u+} , and E_{u-} .

Second, the form factors for in-plane nearest-neighbor pairing contain linear combinations of $\cos k_x$, $\cos k_y$, $\sin k_x$, and $\sin k_y$, where lattice constants are suppressed to simplify notation. These are easily organized by irreps:

$$\cos k_x + \cos k_y \quad A_{1g+}, \quad (17)$$

$$\cos k_x - \cos k_y \quad B_{1g+}, \quad (18)$$

$$(\sin k_x, \sin k_y) \quad E_{u-}. \quad (19)$$

The possible symmetries of in-plane nearest-neighbor pairing states are given in Table IV. Note that all irreps of D_{4h} with positive sign under TR occur in the table.

We next argue why the E_{g+} and E_{u+} pairing states are unlikely to be stable, starting with E_{g+} . The normal-state Hamiltonian contains the basis matrix $h_5 = \tau_z \otimes \sigma_z$ of A_{1u-} symmetry with a prefactor $c_5(\mathbf{k})$, which must be a A_{1u-} basis function. The lowest-order polynomial basis function is $k_x k_y k_z (k_x^2 - k_y^2)$ [21]. h_5 is an Ising spin-orbit-coupling term because it contains σ_z and involves sites on the same sublattice because of the τ_z . The leading

TABLE IV. The possible symmetries of in-plane nearest-neighbor pairing states, which at this stage still involves all irreps of D_{4h} with positive sign under TR. Here, symmetries disfavored by the Hubbard U are marked by an asterisk.

| | A_{1g+} | A_{2g-} | E_{g-} | | A_{1u-} | A_{2u+} | E_{u-} |
|-----------|-------------|-----------|--|----------|-----------|-------------|--|
| A_{1g+} | A_{1g+}^* | | | | | A_{2u+}^* | |
| B_{1g+} | B_{1g+} | | | | | B_{2u+} | |
| E_{u-} | | E_{u+} | $A_{1u+} \oplus A_{2u+}^* \oplus B_{1u+} \oplus B_{2u+}$ | E_{g+} | | | $A_{1g+}^* \oplus A_{2g+} \oplus B_{1g+} \oplus B_{2g+}$ |

A_{1u-} basis function compatible with this is [22]

$$c_5(\mathbf{k}) \propto \sin k_x \sin k_y \sin k_z (\cos k_x - \cos k_y). \quad (20)$$

$c_5(\mathbf{k})$ thus describes coupling between sites with separation vector $(1, 1, 1)$ and symmetry-related ones, where the z -component of 1 refers to one unit cell, i.e., *two* Ce layers. This is thus coupling between next-nearest-neighbor layers and next-nearest neighbors parallel to the planes and is thus expected to be weak. Amin *et al.* [17] also argue that this term is much weaker than the terms discussed in the following.

The basis matrices $h_3 = \tau_z \otimes \sigma_y$ and $h_4 = -\tau_z \otimes \sigma_x$, which form a E_{u-} doublet, also describe spin-orbit coupling within the same sublattice. The leading basis functions are

$$c_3(\mathbf{k}) \sim \sin k_x, \quad (21)$$

$$c_4(\mathbf{k}) \sim \sin k_y \quad (22)$$

and are obviously in-plane nearest-neighbor terms. They are expected to be large compared to the contribution from h_5 . This means that the \mathbf{g} vector describing the spin-orbit coupling has large x - and y -components compared to its z -component, i.e., it is predominantly of Rashba type [17]. For spin-triplet pairing described by an OP with spin dependence $\mathbf{d}(\mathbf{k}) \cdot \boldsymbol{\sigma}$, where $\boldsymbol{\sigma}$ is the vector of Pauli matrices, states with \mathbf{d} vector parallel to \mathbf{g} are favored since they avoid the pair-breaking effect a spin-orbit coupling [23]. Hence, the \mathbf{d} vector also predominantly lies in plane and thus superconducting pairing with a matrix $D(\mathbf{k})$ containing $\tau_z \otimes \sigma_z$ is disfavored in comparison to pairing with $\tau_z \otimes \sigma_x$ and $\tau_z \otimes \sigma_y$. But pairing with E_{g+} symmetry requires the matrix $\tau_z \otimes \sigma_z$ and is thus disfavored.

Conversely, the doublet $(\tau_z \otimes \sigma_y, -\tau_z \otimes \sigma_x)$ is relatively favored. As the previous table shows, this can produce in-plane nearest-neighbor pairing with any one-dimensional even-parity irrep.

Now turning to E_{u+} pairing, we note that in the realm of in-plane pairing it requires the matrix $\tau_0 \otimes \sigma_z$. This matrix differs from $\tau_z \otimes \sigma_z$ only in its dependence on the basis site or interlayer index. There is an analogous relationship between $\tau_0 \otimes \sigma_{x,y}$ and $\tau_z \otimes \sigma_{x,y}$. Since CeRh_2As_2 consists of weakly coupled layers, this change should not strongly affect the stability of states, as noted above. In particular, there is no reason to expect that $\tau_0 \otimes \sigma_z$ becomes favored over $\tau_0 \otimes \sigma_{x,y}$. We conclude that E_{u+} is suppressed in comparison to the other odd-parity pairing states.

Based on the previous discussion, we restrict ourselves to pairing states that involve in-plane nearest-neighbor pairing and have symmetries described by one-dimensional irreps. These states have single-component OPs. To start with, it is useful to write down the corresponding contributions to $D(\mathbf{k})$ (symmetries disfavored by the Hubbard U are again marked by an asterisk):

$$(\cos k_x + \cos k_y) \tau_0 \otimes \sigma_0 \quad A_{1g+}^*, \quad (23)$$

$$(\cos k_x + \cos k_y) \tau_z \otimes \sigma_0 \quad A_{2u+}^*, \quad (24)$$

$$(\cos k_x - \cos k_y) \tau_0 \otimes \sigma_0 \quad B_{1g+}, \quad (25)$$

$$(\cos k_x - \cos k_y) \tau_z \otimes \sigma_0 \quad B_{2u+}, \quad (26)$$

$$\sin(k_x) \tau_z \otimes \sigma_y - \sin(k_y) \tau_z \otimes \sigma_x \quad A_{1g+}^*, \quad (27)$$

$$\sin(k_x) \tau_z \otimes \sigma_y + \sin(k_y) \tau_z \otimes \sigma_x \quad B_{1g+}, \quad (28)$$

$$\sin(k_x) \tau_z \otimes \sigma_x - \sin(k_y) \tau_z \otimes \sigma_y \quad B_{2g+}, \quad (29)$$

$$\sin(k_x) \tau_z \otimes \sigma_x + \sin(k_y) \tau_z \otimes \sigma_y \quad A_{2g+}, \quad (30)$$

$$\sin(k_x) \tau_0 \otimes \sigma_x + \sin(k_y) \tau_0 \otimes \sigma_y \quad A_{1u+}, \quad (31)$$

$$\sin(k_x) \tau_0 \otimes \sigma_x - \sin(k_y) \tau_0 \otimes \sigma_y \quad B_{1u+}, \quad (32)$$

$$\sin(k_x) \tau_0 \otimes \sigma_y + \sin(k_y) \tau_0 \otimes \sigma_x \quad B_{2u+}, \quad (33)$$

$$\sin(k_x) \tau_0 \otimes \sigma_y - \sin(k_y) \tau_0 \otimes \sigma_x \quad A_{2u+}^*. \quad (34)$$

The expressions in Eqs. (27)–(34) result from the reductions $E_{u-} \otimes E_{u-} = A_{1g+} \oplus A_{2g+} \oplus B_{1g+} \oplus B_{2g+}$ and $E_{u-} \otimes E_{g-} = A_{1u+} \oplus A_{2u+} \oplus B_{1u+} \oplus B_{2u+}$ together with the observation that consistently ordered doublets are $(\sin k_x, \sin k_y)$, $(\tau_z \otimes \sigma_y, -\tau_z \otimes \sigma_x)$, and $(\tau_0 \otimes \sigma_x, \tau_0 \otimes \sigma_y)$. In principle, $D(\mathbf{k})$ is a linear combination of these matrix-valued functions of momentum. At the critical temperature T_c , generically only terms belonging to a single irrep will become nonzero, though.

We see that B_{1g+} and B_{2u+} are distinguished from the other irreps in that there are *two* contributions with likely attractive nearest-neighbor pairing interactions. One of the amplitudes describes spin-singlet pairing (σ_0) and the other spin-triplet pairing ($\sigma_{x,y}$). On the other hand, the remaining irreps A_{2g+} , A_{1u+} , B_{2g+} , and B_{1u+} only contain a nearest-neighbor spin-triplet contribution. Observing that spin-singlet pairing is much more common than spin-triplet pairing, unless they coexist due to symmetry, it is natural to assume that the pairing interactions in the spin-singlet channels are stronger. We conclude that the B_{1g+} and B_{2u+} pairing states are favored over the others.

Which one of these two states wins? To answer this, we recall that due to the weakly coupled layers in CeRh_2As_2 , pairing states that only differ in the sign under inversion, i.e., in containing τ_0 vs. τ_z , are close in energy. We call

TABLE V. Possible partner states for single-component, in-plane, nearest-neighbor pairing. The states are subdivided by their transformation behavior under inversion, i.e., by containing τ_0 vs. τ_z .

| favored (0 junctions) | | disfavored (π junctions) | |
|---|-------------|---|-------------|
| $(\cos k_x + \cos k_y) \tau_0 \otimes \sigma_0$ | A_{1g+}^* | $(\cos k_x + \cos k_y) \tau_z \otimes \sigma_0$ | A_{2u+}^* |
| $(\cos k_x - \cos k_y) \tau_0 \otimes \sigma_0$ | B_{1g+} | $(\cos k_x - \cos k_y) \tau_z \otimes \sigma_0$ | B_{2u+} |
| $\sin(k_x) \tau_0 \otimes \sigma_x + \sin(k_y) \tau_0 \otimes \sigma_y$ | A_{1u+} | $\sin(k_x) \tau_z \otimes \sigma_x + \sin(k_y) \tau_z \otimes \sigma_y$ | A_{2g+} |
| $\sin(k_x) \tau_0 \otimes \sigma_y - \sin(k_y) \tau_0 \otimes \sigma_x$ | A_{2u+}^* | $\sin(k_x) \tau_z \otimes \sigma_y - \sin(k_y) \tau_z \otimes \sigma_x$ | A_{1g+}^* |
| $\sin(k_x) \tau_0 \otimes \sigma_x - \sin(k_y) \tau_0 \otimes \sigma_y$ | B_{1u+} | $\sin(k_x) \tau_z \otimes \sigma_x - \sin(k_y) \tau_z \otimes \sigma_y$ | B_{2g+} |
| $\sin(k_x) \tau_0 \otimes \sigma_y + \sin(k_y) \tau_0 \otimes \sigma_x$ | B_{2u+} | $\sin(k_x) \tau_z \otimes \sigma_y + \sin(k_y) \tau_z \otimes \sigma_x$ | B_{1g+} |

such states “partner states.” Weakly coupled layers can be understood as two-dimensional superconductors with Josephson junctions connecting them. There is nothing about CeRh_2As_2 that indicates that these should be π junctions, i.e., favoring a sign change of the pairing amplitude. In particular, there are no magnetic ions between the layers. We conclude that the pairing states containing τ_0 are favored over their partners containing τ_z [24]. The partner states are listed in Table V. The free energy of a Josephson junction is proportional to $\cos \Delta\phi$ to leading order, where $\Delta\phi$ is the phase difference between the two superconductors. This implies that for 0 junctions the first partner of the above pairs minimizes the free energy, whereas the second partner maximizes it. We conclude that any state that only appears in the right-hand (π -junction) column of Table V is not even a local minimum of the free energy and is thus unstable towards its partner state.

Hence, if spin-singlet pairing is stronger than spin-triplet pairing, as we argued above, B_{1g+} is favored over B_{2u+} . The chain of arguments up to this point suggests that the low-field pairing state of CeRh_2As_2 has B_{1g+} symmetry. Our result is consistent with the $d_{x^2-y^2}$ -pairing state recently proposed by Amin *et al.* [17]. In that work, Kramers’ degenerate magnetic order, i.e., magnetic order that breaks inversion and TR symmetry but preserves their product, and its interplay with superconductivity are considered. We address the magnetic order in the following section. The closely competing B_{1g} and B_{2u} states are also found by Lee *et al.* [25] from a renormalization-group analysis of a $\mathbf{k} \cdot \mathbf{p}$ model centered at the X point. However, Lee *et al.* [25] find that the B_{2u} state is stabilized in large parameter regions. Pairing states that are insensitive to the local interaction have also been found by Nogaki and Yanase [26] using the fluctuation exchange approximation, by Nally and Brydon [9] from a t - J model treated within a mean-field approximation, and by Lee *et al.* [25] with a parquet renormalization-group approach.

IV. MAGNETIC ORDERING

Magnetic ordering in CeRh_2As_2 was reported for the first time from NQR and NMR experiments [8, 13]. Here,

the onset of magnetism remarkably was found to occur below the superconducting transition, i.e., at a Néel temperature $T_N < T_c$. These measurements are most suited to identify the symmetry of the magnetic order, as discussed in the following subsection. The “ T_0 order” or phase I mentioned in Sec. I was interpreted in terms of quadrupolar order [10, 12]. Recently, this scenario has been challenged by μSR studies; Khim *et al.* [15] suggest a magnetic dipolar character of phase I.

A. Magnetic order parameters from NQR and NMR

In this section, we discuss the possible magnetic OPs in view of the NQR experiments by Kibune *et al.* [13] and NMR experiments by Ogata *et al.* [8, 14]. There is no experimental indication that the magnetic order breaks translational symmetry and we here restrict ourselves to magnetic orders that preserve this symmetry. The NQR and NMR experiments are sensitive to the local magnetic field at As positions. There are two inequivalent positions, see Fig. 1: As(1) forms a square lattice in the middle between two Ce layers. The As(1) square lattice is rotated by 45° relative to the Ce square lattice and contains twice as many sites. As(2) is vertically aligned with Ce sites and does not lie in the middle between Ce layers. The central result of [13] is that in the absence of an applied magnetic field, the local magnetic field at the As(1) site is consistent with zero, whereas the local field at As(2) is clearly nonzero, as shown by a strong broadening of the NQR peak. The NMR experiments [8] are consistent with this result.

It is natural to attribute the magnetic order to the Ce f moments. Alternatively, it may be the consequence of TR-symmetry-breaking superconductivity, which is carried by electrons at the Fermi energy, which also have a high Ce f -orbital weight. Here, we consider magnetic moments at the Ce sites. We first consider a single Ce double layer with the As(1) layer in the center. The absence of a magnetic field at the As(1) sites strongly constrains the possible magnetic moments at the Ce sites. These moments can be decomposed into components along the lattice axes. There are three linearly independent possible orders, which are shown in Fig. 2. All linear combina-

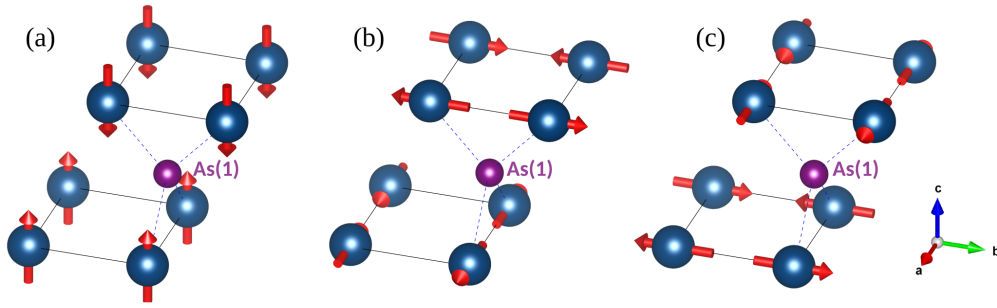


FIG. 2. The three linearly independent translationally invariant magnetic orders consistent with the absence of a magnetic field at the As(1) sites. All linear combination are also compatible with the NQR experiments [13]. Configurations (b) and (c) are degenerate.

tion of these configurations are also compatible with the NQR experiments. The second and third configuration are degenerate.

By symmetry, the relative orders of the Ce moments in all pairs of Ce layers that have the same distance from a As(1) layer are restricted in the same manner [27]. This forces the moments in Ce double layers with a separation of *two* lattice constants along the *c*-axis to be aligned in parallel. Numbering the double layers by $n_c \in \mathbb{Z}$, we thus find that the relative orientation of moments in even-numbered and odd-numbered double layers are not constrained by the NQR results [28]. The natural magnetic unit cell thus comprises two double layers in the *z*-direction.

A double layer with nearest-neighbor interactions within the planes and between the planes and without magnetic anisotropy is equivalent to the J_1 - J_2 -Heisenberg model on the square lattice. While the configuration with antiparallel ferromagnetic (FM) layers in Fig. 2(a) is quite natural for this model, the *noncollinear* configurations in Figs. 2(b) and 2(c) do not occur as equilibrium states. Below, we analyze the symmetry of possible magnetic states that do not break translational symmetry, which applies to the first configuration but not to the other two. If one allows for translational symmetry to be broken the nonsymmorphic space group $P4/nmm$ leads to the appearance of irreps that mix even and odd parity, as recently studied by Szabó and Ramires [29] for the simplest case that the unit cell is doubled.

The magnetic field at the As(1) and As(2) sites can be decomposed into components along the lattice axes. These components can be classified according to irreps, by checking the action of the operations from D_{4h} on the local fields. Of course, the local field could, in principle, point in any direction but if it has in-plane and *c*-axis components this would imply a state with mixed irreps, which is not expected generically. The irreps for the As(1) and As(2) sites are shown in Fig. 3.

We see that the *only* magnetic symmetry consistent with zero field at As(1) and nonzero field at As(2) is A_{1u-} , i.e., an out-of-plane AFM order [30]. This proposed A_{1u-} order is shown in Fig. 4. Szabó and Ramires

[29] have come to the same conclusion. Note that A_{1u-} magnetic order is odd under inversion and under TR but even under their product. This is the case considered by Amin *et al.* [17]. On the other hand, the out-of-plane Néel vector of the A_{1u-} order seems to contradict the experimentally favored easy plane anisotropy [31]. However, new NMR results [14] indicate that the moment is indeed out of plane, consistent with A_{1u-} symmetry.

As noted above, the magnetic order is likely predominantly carried by the Ce atoms. The symmetry classification is analogous to the case of the As(2) sites. The result is again that the only pure irrep consistent with the NQR results is A_{1u-} , see the left sketch in Fig. 3(a) in [13]. Note that the right sketch in Fig. 3(a) [13] shows magnetic order that breaks translational symmetry. This is a spiral state, as is best seen by following the $[111]$ direction. It is neither even nor odd under inversion at *any* center and is even under TR. It is thus not a pure-irrep order but mixes E_{g+} and E_{u+} . Actually, for in-plane Ce moments, the NQR results [13] do not constrain the rotation of these moments between Ce sites separated by layers containing As(2) sites. There are thus variants of Fig. 3(a) [13], right part, that also explain the data but have different dependence of the orientation of moments as a function of *z*. These magnetic orders are not more natural than the above mixture of E_{g+} and E_{u+} .

More recent NMR experiments [8] shed additional light on the magnetic state. The results still find a transition to a TR-symmetry-breaking state in zero field, at a temperature below the superconducting T_c [13]. In addition, this magnetic transition is now followed to nonzero magnetic fields along the *z*-direction [8]. Its critical temperature decreases with increasing B_z but slightly less so than the superconducting T_c . The NMR results are consistent with the magnetic transition line ending where it reaches the first-order superconductor-to-superconductor transition at about 4 T, which is the interpretation given by the authors [8].

As noted above, recent μ SR experiments [15] suggest that phase I in the normal state has magnetic dipolar character, i.e., that $T_N > T_c$. The internal magnetic field seen by μ SR is continuous through T_c , hence the mag-

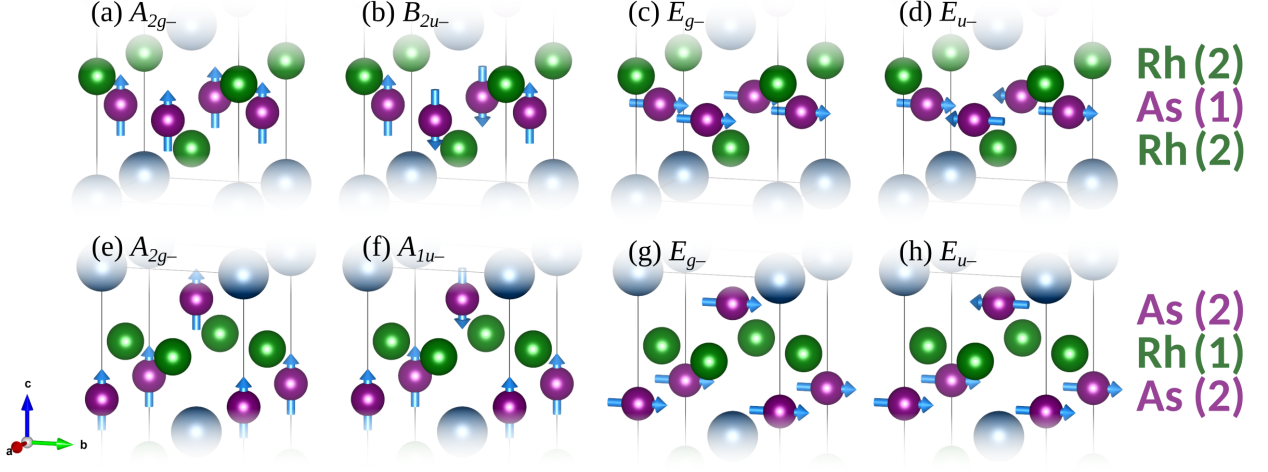


FIG. 3. Irreducible representations of possible magnetic orders for (a)–(d) the As(1) and (e)–(h) the As(2) sites: (a), (e) out-of-plane FM, (b), (f) out-of-plane AFM, (c), (g) in-plane FM, and (d), (h) in-plane AFM.

netic order is likely of the same type above and below T_c . Moreover, the internal field is found to be roughly temperature independent below T_c instead of rising further upon cooling [15]. This indicates that magnetic order and superconductivity are coupled and compete with each other [15]. Recently, the magnetic transition could be observed within the high-field superconducting phase, where the critical field is also roughly temperature independent [32]. The origin of the distinct magnetic ordering temperatures might be different quality of older and newer samples. Another possibility is that the magnetic order is not static but has a certain finite timescale. In such a situation, the different timescales of the experimental probes lead to distinct critical temperatures [15]. We consider both the cases $T_N > T_c$ and $T_N < T_c$ in our analysis.

Note that the application of a uniform magnetic field leads to a FM contribution in addition to the out-of-plane AFM A_{1u-} order. Such a field can be decomposed into a z -component B_z , which transforms according to A_{2g-} ,

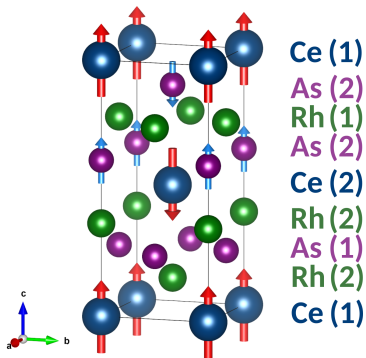


FIG. 4. Proposed out-of-plane AFM A_{1u-} order of CeRh_2As_2 with zero field at As(1) and nonzero field at As(2) sites.

and in-plane components (B_x, B_y) , which transform according to E_{g-} . Thus, the expected FM OP symmetries are A_{2g-} and E_{g-} , respectively. One could speak of a canted AFM state in this case. Compared to the pure A_{1u-} state, this would lead to an increased line width also at the As(1) sites for finite fields. The comparison of out-of-plane NMR measurements [8] with recent in-plane results [14] suggests that this effect could be especially pronounced for fields within the plane, even at low field amplitudes. This could contribute to the explanation for why a significant site-dependent broadening is observed for $\mathbf{B} \parallel [001]$ [8] but not for $\mathbf{B} \parallel [110]$ [14]. However, in this work we focus on the primary AFM A_{1u-} OP, which we expect to be the most relevant contribution for the purpose of understanding the superconducting phase transitions.

B. Coexistence of superconducting and magnetic order parameters

If superconductivity and magnetic order coexist for zero applied field and the two order parameters do not belong to the same irrep, then a secondary superconducting order parameter is induced. In the language of Landau theory, there are allowed trilinear terms of the form [29]

$$M i (\Delta_1^* \Delta_2 - \Delta_2^* \Delta_1), \quad (35)$$

where M is the magnetic OP, Δ_1 and Δ_2 are superconducting OPs, and the term must have A_{1g+} , i.e., full, symmetry. We denote the irreps of the three OPs by Γ_M , Γ_1 , and Γ_2 . Since the likely primary superconducting OP and the magnetic OP were found to belong to one-dimensional irreps we restrict ourselves to this situation. It is then easy to see that the irrep of the induced OP is also one dimensional. Any symmetry-allowed term

must then satisfy

$$A_{1g+} = \Gamma_M \otimes A_{1g-} \otimes \Gamma_1 \otimes \Gamma_2,$$

where the additional factor A_{1g-} (odd under TR, otherwise trivial) appears because $\Delta_1^* \Delta_2 - \Delta_2^* \Delta_1$ is odd under TR since it maps to $\Delta_1 \Delta_2^* - \Delta_2 \Delta_1^* = -(\Delta_1^* \Delta_2 - \Delta_2^* \Delta_1)$. It follows that the induced superconducting OP must belong to the irrep

$$\Gamma_2 = A_{1g-} \otimes \Gamma_M \otimes \Gamma_1. \quad (36)$$

As discussed above, we propose $\Gamma_M = A_{1u-}$ and $\Gamma_1 = B_{1g+}$. Hence, we obtain $\Gamma_2 = B_{1u+}$ for the induced OP.

An alternative view leading to the same Eq. (35) is to think of the two superconducting OPs as primary. Since they have different symmetry they generically appear at different critical temperatures. But when they coexist, a magnetic order parameter belonging to the irrep $\Gamma_M = A_{1g-} \otimes \Gamma_1 \otimes \Gamma_2$ is automatically induced. Such a scenario cannot easily explain the case of $T_N > T_c$, though.

V. FIELD-INDUCED SUPERCONDUCTING ORDERS AND PAIR BREAKING

In this section, we investigate the effects of applying a magnetic field in the presence of superconducting order, where the field generically induces further superconducting OPs. In the bulk, this only happens if the field actually penetrates the sample, i.e., in the vortex phase. The symmetry of the induced OP can be determined in the standard way using product representations. We elaborate on this below. Moreover, the magnetic field can suppress and eventually destroy superconducting condensates, which can happen due to orbital and Pauli limiting. Pauli (paramagnetic) limiting is central for the understanding of the superconductor-to-superconductor transition and is discussed in Sec. V C.

A. Out-of-plane field

We first consider the case of a field in the z -direction, which transforms according to A_{2g-} . In Landau theory, and assuming that the irreps of the superconducting states are one dimensional, the induction of another OP is described by a symmetry-allowed trilinear term

$$F_3 = B_z i (\Delta_1^* \Delta_2 - \Delta_2^* \Delta_1). \quad (37)$$

The irrep of the induced superconducting OP is

$$\Gamma_2 = A_{2g-} \otimes A_{1g-} \otimes \Gamma_1 = A_{2g+} \otimes \Gamma_1, \quad (38)$$

where the additional factor A_{1g-} appears because $\Delta_1^* \Delta_2 - \Delta_2^* \Delta_1$ is odd under TR, see Sec. IV B. Hence, for $\Gamma_1 = B_{1g+}$, the field induces B_{2g+} pairing.

When two superconducting OPs of symmetries B_{1g+} and B_{1u+} coexist, as argued in Sec. IV B, the applied

field induces two additional OPs B_{2g+} and B_{2u+} . For weak applied field, the induced OPs will be linear in B_z and hence small.

One of the most striking properties of CeRh_2As_2 is the first-order superconductor-to-superconductor transition at an applied magnetic field of about 4 T in the z -direction. This field is likely far above the lower critical field [8]. Hence, the magnetic field penetrates in the form of overlapping vortices. In the high-field phase we again get a pair (or possibly two pairs) of superconducting OPs related by Eq. (38).

The arguments stated above concerning (a) the Hubbard repulsion U , (b) the weakness of pairing in the two-component E_g and E_u channels, and (c) the preference for 0 junctions between layers are not strongly affected by a magnetic field in the z -direction. On the other hand, for sufficiently strong magnetic field, spin-singlet pairing will no longer be favored over spin-triplet pairing. The reason is related to Eq. (37): The free energy will be lowered linearly in B_z if two suitable superconducting OPs coexist. They must satisfy Eq. (38) and have a phase difference of $\pm\pi/2$ (the sign depends on the sign of B_z).

A microscopic consideration is helpful at this point. We consider the gap product

$$\Delta \Delta^\dagger = D U_T U_T^\dagger D^\dagger = D D^\dagger \quad (39)$$

since its TR-odd part is a magnetic OP [33, 34]. We assume the two pairing amplitudes to be Δ_1 and $i\Delta_2$ with $\Delta_1, \Delta_2 \in \mathbb{R}$. One finds that the TR-odd part of $\Delta \Delta^\dagger$ is proportional to the commutator of the pairing matrices. Hence, spin-singlet parts cannot contribute since they only occur with the matrices $\tau_0 \otimes \sigma_0$ and $\tau_z \otimes \sigma_0$ in Eqs. (23)–(26), which commute with all matrices in Eqs. (23)–(34). Hence, only spin-triplet states contribute to the TR-odd part of the gap product and thus only they couple to B_z .

Equation (38) implies that the field B_z favors pairs of OPs with irreps Γ_1 and Γ_2 satisfying

$$\Gamma_1 \otimes \Gamma_2 = A_{2g+}, \quad (40)$$

where we still assume one-dimensional irreps. The possible pairs are

$$\begin{aligned} A_{2g+} &= A_{1g+} \otimes A_{2g+} = B_{1g+} \otimes B_{2g+} \\ &= A_{1u+} \otimes A_{2u+} = B_{1u+} \otimes B_{2u+}. \end{aligned} \quad (41)$$

All eight one-component OPs have a spin-triplet contribution and thus all four combinations can gain free energy linearly in a B_z field.

Applying the same reasoning as above, we can assess the four possibilities in Eq. (41) as follows: The products $A_{1g+} \otimes A_{2g+}$ and $A_{1u+} \otimes A_{2u+}$ both involve an OP that is suppressed by the Hubbard repulsion. The B irreps are not affected by the Hubbard repulsion. Among these, the combination $B_{1u+} \otimes B_{2u+}$ is favored over $B_{1g+} \otimes B_{2g+}$ because the term coupling to the B_z field involves 0 junctions between layers in both B_{1u+} and B_{2u+} . The analogous term for $B_{1g+} \otimes B_{2g+}$ involves π junctions in both

OPs and is therefore expected to be unstable towards B_{1u+} and B_{2u+} .

We have argued above that in the absence of an applied magnetic field, B_{1g+} pairing is favored, with a possibly coexisting B_{1u+} superconducting OP (and thus AFM order). The B_z field then induces B_{2g+} (and possibly B_{2u+}) pairing. The emerging scenario is thus that the free-energy gain through the coexistence of the triplet, sublattice-even pairing symmetries B_{1u+} and B_{2u+} makes these states dominant above a sufficiently strong magnetic field B_z , where the first-order transition takes place. Note that if B_{1u+} already exists as a secondary OP in the low-field phase and becomes one of the primary OPs in the high-field phase, then there is no difference in symmetry between the low-field and the high-field phase. This begs the question of why a phase transition takes place. We will return to this point below.

Machida [35] has proposed a magnetic mechanism for the superconductor-to-superconductor transition in a field B_z : It is essentially a spin-flop transition of an antiferromagnet of local Ce moments in a magnetic field applied in parallel to the low-field Néel vector. In this scenario, the low-field superconducting phase has AFM order with Néel vector along the z -axis, which is consistent with the A_{1u-} magnetic order discussed above. At the first-order transition, the Néel vector jumps into the xy plane and the Ce moments are canted by the field, leading to a nonzero magnetization [35]. Such a magnetically driven scenario could not explain a situation where the magnetic transition meets the first-order superconductor-to-superconductor phase transition below T_c [8].

B. In-plane field

The in-plane field components (B_x, B_y) transform according to E_{g-} . This requires a superconducting OP belonging to a two-dimensional irrep to construct a trilinear term. The two irreps Γ_1 and Γ_2 of the superconducting OPs must be such that the product $E_{g-} \otimes A_{1g-} \otimes \Gamma_1 \otimes \Gamma_2 = E_{g+} \otimes \Gamma_1 \otimes \Gamma_2$ contains A_{1g+} . The relevant products are given in Table VI.

The structure is rather simple because for D_{4h} , the product of two two-dimensional irreps only contains one-dimensional irreps. We see that starting from a primary superconducting OP corresponding to a one-dimensional irrep, a secondary E_{g+} or E_{u+} OP is induced if the primary pairing is of even or odd parity, respectively. The allowed trilinear terms are the following, here indexed by Γ_1 :

$$F_{3,A_{1g+}} = F_{3,A_{1u+}} = i [\Delta_1^* (B_x \Delta_{2x} + B_y \Delta_{2y}) - \Delta_1 (B_x \Delta_{2x}^* + B_y \Delta_{2y}^*)], \quad (42)$$

$$F_{3,A_{2g+}} = F_{3,A_{2u+}} = i [\Delta_1^* (B_x \Delta_{2y} - B_y \Delta_{2x}) - \Delta_1 (B_x \Delta_{2y}^* - B_y \Delta_{2x}^*)], \quad (43)$$

$$F_{3,B_{1g+}} = F_{3,B_{1u+}} = i [\Delta_1^* (B_x \Delta_{2x} - B_y \Delta_{2y}) - \Delta_1 (B_x \Delta_{2x}^* - B_y \Delta_{2y}^*)], \quad (44)$$

$$F_{3,B_{2g+}} = F_{3,B_{2u+}} = i [\Delta_1^* (B_x \Delta_{2y} + B_y \Delta_{2x}) - \Delta_1 (B_x \Delta_{2y}^* + B_y \Delta_{2x}^*)], \quad (45)$$

where the two-dimensional OP is written as $(\Delta_{2x}, \Delta_{2y})$ [36].

We have seen in Secs. II and III that in-plane nearest-neighbor E_{g+} and E_{u+} pairing states are disfavored by spin-orbit coupling. The relevant OPs are

$$(\sin k_x, \sin k_y) \tau_z \otimes \sigma_z \quad E_{g+}, \quad (46)$$

$$(\sin k_y, -\sin k_x) \tau_0 \otimes \sigma_z \quad E_{u+}. \quad (47)$$

They both describe pure spin-triplet pairing and can thus realize the trilinear terms above since all A and B OP also contain spin-triplet contributions. Hence, for all one-dimensional OPs, the in-plane field induces a two-dimensional OP. More precisely, the field induces one component of the two-dimensional OP, namely the one that can be said to be parallel to the field.

For zero-field B_{1g+} and potentially coexisting B_{1u+} OPs, the in-plane field induces E_{g+} and E_{u+} pairing, respectively. The relevant coupling terms in Landau theory are given by Eq. (44). In the microscopic picture, both are dominated by a term belonging to the z -component of the spin-triplet-pairing \mathbf{d} vector. Following Frigeri *et al.* [23], for this component, the predominant in-plane spin-orbit coupling is pair breaking. This is different for the B OPs induced by a magnetic field in the z -direction. It is thus expected that the induced E_{g+} and E_{u+} OPs are not very helpful in stabilizing the superconducting state.

C. Pauli limiting

The most commonly discussed mechanism in the context of the superconductor-to-superconductor transition is Pauli limiting [5, 7–9, 17, 35, 37, 38], i.e., the destruction of a superconducting state by an applied magnetic field due to the Zeeman splitting of the bands [39–41].

TABLE VI. The relevant products of two irreducible representations Γ_1 and Γ_2 of the superconducting OPs for in-plane fields such that the product $E_{g+} \otimes \Gamma_1 \otimes \Gamma_2$ contains A_{1g+} . Products obtained by interchanging Γ_1 and Γ_2 have been omitted.

| Γ_1 | Γ_2 | $E_{g+} \otimes \Gamma_1 \otimes \Gamma_2$ |
|------------|------------|--|
| A_{1g+} | E_{g+} | |
| A_{2g+} | E_{g+} | |
| B_{1g+} | E_{g+} | |
| B_{2g+} | E_{g+} | |
| A_{1u+} | E_{u+} | $A_{1g+} \oplus A_{2g+} \oplus B_{1g+} \oplus B_{2g+}$ |
| A_{2u+} | E_{u+} | |
| B_{1u+} | E_{u+} | |
| B_{2u+} | E_{u+} | |

For a B_z field, the bands in the normal state split into spin- \uparrow and spin- \downarrow bands and thus the Fermi surface splits correspondingly. Consequently, superconducting states with Cooper pairs made up of \uparrow and \downarrow electrons of opposite momenta can gain less free energy and eventually become unstable towards the normal state or other superconducting states. One way a system could nevertheless gain free energy in a superconducting state is by pairing \uparrow and \downarrow electrons at the Fermi energy but then necessarily at different momenta. So far, there is no direct evidence for such Fulde–Ferrell–Larkin–Ovchinnikov states [42, 43] in CeRh_2As_2 . However, an inhomogeneous state has recently been invoked as a way to explain a discrepancy between the Pauli limiting field obtained by extrapolating Knight shift data to zero temperature and the actual upper critical field, for the high-field phase [8].

The above implies that Pauli limiting for a B_z field is only effective for Cooper pairs made up of electrons with opposite spins. These are states for which the pairing matrix $\Delta(\mathbf{k})$ contains σ_x or σ_y . We split off the unitary part of the TR operator according to Eq. (16), $\Delta(\mathbf{k}) = D(\mathbf{k})(\tau_0 \otimes i\sigma_y)$. Hence, for Pauli-limited states, $D(\mathbf{k})$ contains σ_0 (spin-singlet pairing) or σ_z (spin-triplet pairing with \mathbf{d} vector along the z -direction). Conversely, superconducting states avoid Pauli limiting if $D(\mathbf{k})$ contains only σ_x or σ_y (spin-triplet pairing with \mathbf{d} vector in the xy plane).

The relevant observation for CeRh_2As_2 is that the high-field phase is not or perhaps extremely weakly Pauli limited, while the low-field state still shows significantly weaker Pauli limiting than expected for a conventional superconductor [5]. The arguments in the previous sections did not refer to Pauli limiting at all. It is thus necessary to check how Pauli limiting changes the picture.

The proposed primary B_{1g+} pairing at low field has two contributions from nearest-neighbor pairing: $(\cos k_x - \cos k_y) \tau_0 \otimes \sigma_0$ and $\sin(k_x) \tau_z \otimes \sigma_y + \sin(k_y) \tau_z \otimes \sigma_x$. The first involves pairing of opposite spins and is thus susceptible to Pauli limiting, whereas the second involves pairing of equal spins and is not affected by Pauli limiting. It is natural to expect that the presence of the second component increases the critical field somewhat. However, it is an unfavorable state since it involves π junctions between the layers. It is not obvious that this symmetry-allowed but disfavored pairing is sufficient to quantitatively explain the enhanced critical field of the low-field phase. Note that here the induced B_{2g+} spin-triplet pairing will also contribute.

The possible secondary B_{1u+} pairing has the nearest-neighbor contribution $\sin(k_x) \tau_0 \otimes \sigma_x - \sin(k_y) \tau_0 \otimes \sigma_y$, which avoids Pauli limiting. Its presence thus could help to explain the enhancement of the critical field of the low-field phase, though not in case of $T_N < T_c$, where it does not exist above the magnetic phase transition.

For the high-field phase, we have proposed the coexistence of dominant B_{1u+} and induced B_{2u+} pairing. Both have spin-triplet contributions that avoid Pauli limiting

and B_{2u+} in addition has a spin-singlet contribution, which is Pauli limited. Since the magnetic field is larger than the Pauli-limiting field for conventional spin-singlet superconductors, this contribution is likely strongly suppressed. Hence, the critical field of the high-field phase is expected to be well described by only considering orbital limiting.

We thus find that the inclusion of Pauli limiting does not overturn our scenario but refines it. The main additional insight concerns the low-field phase: Previously, we had argued that the low-field phase has two contributions, singlet pairing that does not couple linearly to the B_z field and triplet pairing that is favored by the B_z field but less so than the high-field phase, which thus eventually takes over. Now we see that the low-field spin-singlet pairing is actually weakened by Pauli limiting.

The dominant high-field state favored by our considerations, which consist of spin-triplet, orbitally even B_{1u+} and B_{2u+} pairing with a $\pi/2$ phase difference, is in contradiction to the spin-singlet pair density wave (PDW) suggested by Ogata *et al.* [8]. By PDW, the authors mean an intra-unit-cell modulation by a Pauli matrix τ_z for the sublattice degree of freedom, not a long-wave-length modulation of the superconducting OP. A spin-singlet pairing state in strong applied field appears highly unlikely because it is susceptible to Pauli limiting.

We now discuss the case of the magnetic field being oriented within the basal plane. In analogy to the previous discussion, Pauli limiting occurs for states for which $D(\mathbf{k})$ contains σ_0 or $\hat{B}_x \sigma_x + \hat{B}_y \sigma_y$, where $(\hat{B}_x, \hat{B}_y, 0)$ is the unit vector in the direction of the magnetic field. Hence, while the B_{1g+} and B_{1u+} OPs are Pauli limited for in-plane field, the E_{g+} and E_{u+} OPs are not. This is not expected to stabilize superconductivity at high in-plane fields because (a) the trilinear terms are suppressed by Pauli limiting of the one-dimensional OPs and (b) the E_{g+} and E_{u+} OPs are intrinsically disfavored.

One might ask why the in-plane field does not cause a first-order transition to a state that avoids Pauli limiting. Such a scenario would require two superconducting OPs belonging to irreps Γ_1 and Γ_2 such that (a) $E_{g+} \otimes \Gamma_1 \otimes \Gamma_2$ contains A_{1g+} and (b) for both OPs, $D(\mathbf{k})$ contains a term that is proportional to either $\hat{B}_y \sigma_x - \hat{B}_x \sigma_y$ (the in-plane component orthogonal to the in-plane field) or σ_z . One of the OPs has to be one dimensional, the other two dimensional. As seen above, for nearest-neighbor pairing, the former never contain σ_z , whereas the latter always contain σ_z . Hence, we have to find one-dimensional OPs for which $D(\mathbf{k})$ is proportional to $\hat{B}_y \sigma_x - \hat{B}_x \sigma_y$. However, Eqs. (27)–(34) show that this is never realized since for all one-dimensional OPs the coefficients of σ_x and σ_y are distinct functions of \mathbf{k} . We conclude that, at least for nearest-neighbor pairing, CeRh_2As_2 cannot avoid Pauli limiting for in-plane magnetic fields.

D. Implications of Knight shift data

Recent NMR data [8] showed clear signatures of the superconducting transitions in the Knight shift, which has implications for the superconducting states. For both the low-field and a single field for the high-field phase ($B_z = 4.5$ T, slightly above the first-order transition), the Knight shift shows a kink at T_c and a decrease below T_c with decreasing temperature. The magnetic transition in the low-field superconducting phase is invisible in the Knight shift for As(1), while the Knight shift for As(2) cannot be determined below this transition because of the very large line width. The absence of a signature for As(1) is consistent with an A_{1u-} magnetic OP.

Generally, a temperature-dependent Knight shift below T_c indicates a spin-singlet state or a spin-triplet state with \mathbf{d} vector along the z -direction, for a B_z field. Conversely, a spin-triplet state with in-plane \mathbf{d} vector is expected to lead to a temperature-independent Knight shift since there is no energy gap suppressing spin flips [44]. Ogata *et al.* [8] conclude that both superconducting phases are spin-singlet states. The possibility of a spin-triplet state with \mathbf{d} vector along the z -direction is not considered. Recall that we argued above that the out-of-plane component of the \mathbf{d} vector should indeed be small. A primary B_{1g+} superconducting OP in the low-field phase, which should be dominated by a spin-singlet contribution, see Eq. (25), is potentially consistent with the authors' interpretation. On the other hand, we have proposed coexisting B_{1u+} and B_{2u+} states in the high-field phase. The latter contains a spin-singlet contribution, which is expected to be strongly suppressed at the relevant fields above 4 T. The remaining, dominantly spin-triplet states with \mathbf{d} vectors in the xy plane are inconsistent with the authors' interpretation.

However, regardless of whether a proposed spin-singlet state in the high-field regime has B_{2u+} or some other symmetry, one has to explain how this state (mostly) avoids Pauli limiting. Moreover, not only is it unclear how a spin-singlet state can avoid Pauli limiting, the upper critical field is also inconsistent with the expectations based on the Knight-shift data. The Pauli-limiting field estimated from the As(1) Knight shift at 4.5 T is 4.8 T [8], much smaller than the actual upper critical field of about 14 T. Ogata *et al.* [8] invoke a spatially modulated superconducting state in order to resolve the problem. We instead suggest that the high-field phase might still contain a sizable spin-singlet contribution at $B_z = 4.5$ T, explaining the temperature-dependent Knight shift, and that this contribution dies out for increasing field, leaving only the spin-triplet contribution, which is unaffected by Pauli limiting, explaining the high upper critical field. It is still nontrivial to understand sizable spin-singlet pairing at 4.5 T but this scenario does not require significant spin-singlet pairing up to 14 T, which Ogata *et al.* [8] have to assume. It remains to be seen whether this explanation can work quantitatively under realistic assumptions.

VI. LANDAU FREE-ENERGY EXPANSION

In this section, we construct a phenomenological Landau expansion of the free energy and focus on the minimal set of necessary ingredients, i.e., the primary single-component OPs Δ_1 , Δ_2 , and M . Based on this theory, we are able to generate phase diagrams that agree with state-of-the-art experimental observations [5, 6, 8, 10, 11, 13, 15, 32] and to analyze the complex interplay between magnetism, superconductivity, and an applied magnetic field in CeRh₂As₂.

The expansion up to fourth order in symmetry-allowed products of Δ_1 (irrep B_{1g+}), Δ_2 (B_{1u+}), M (A_{1u-}), B_z (A_{2g-}), and (B_x, B_y) (E_{g-}) can be written as

$$F = F_{\text{pure}} + F_{\text{mixed}} + F_{\text{field}}, \quad (48)$$

with

$$F_{\text{pure}} = \alpha_1 \Delta_1^* \Delta_1 + \alpha_2 \Delta_2^* \Delta_2 + \alpha_M M^2 + \beta_1 (\Delta_1^* \Delta_1)^2 + \beta_2 (\Delta_2^* \Delta_2)^2 + \beta_M M^4, \quad (49)$$

$$F_{\text{mixed}} = \gamma_{12} \Delta_1^* \Delta_1 \Delta_2^* \Delta_2 + \gamma_{1M} \Delta_1^* \Delta_1 M^2 + \gamma_{2M} \Delta_2^* \Delta_2 M^2 + \delta_{12M} M i (\Delta_1^* \Delta_2 - \Delta_2^* \Delta_1), \quad (50)$$

$$F_{\text{field}} = (B_x^2 + B_y^2) (\lambda_1^{xy} \Delta_1^* \Delta_1 + \lambda_2^{xy} \Delta_2^* \Delta_2 + \lambda_M^{xy} M^2) + B_z^2 (\lambda_1^z \Delta_1^* \Delta_1 + \lambda_2^z \Delta_2^* \Delta_2 + \lambda_M^z M^2). \quad (51)$$

Here, F_{pure} contains standard terms of single OPs and the second-order coefficients are expanded to linear order in temperature,

$$\alpha_1 = \alpha'_1 (T - T_{c1}), \quad (52)$$

$$\alpha_2 = \alpha'_2 (T - T_{c2}), \quad (53)$$

$$\alpha_M = \alpha'_M (T - T_M), \quad (54)$$

with $\alpha'_1, \alpha'_2, \alpha'_M > 0$, i.e., the second-order terms stabilize the corresponding OPs below their (bare) critical temperatures. Note that the actual critical temperature T_c of superconductivity as well as the actual Néel temperature T_N do not necessarily coincide with the temperatures T_{c1} , T_{c2} and T_M in Eqs. (52)–(54). Generally, we find $T_c \leq T_{c1}$ at $\mathbf{B} = 0$ since in the case of $T_N > T_c$ magnetism slightly suppresses the superconducting order and shifts T_c below T_{c1} . For the same reason we have $T_N \leq T_M$, due to the suppression of magnetism by pre-existing superconductivity for $T_N < T_c$. In order for the free energy to be bounded, positive fourth-order terms are included.

In F_{mixed} , we introduce terms containing different OPs, i.e., couplings between ordered phases. The standard bi-quadratic terms carry coefficients γ_s . We want to highlight the distinctiveness of the trilinear δ -term, which guarantees that the third OP is automatically stabilized once the other two are present, see Eq. (35) and the accompanying discussion above. This trilinear coupling will turn out to be of crucial importance since it enables, for example, the symmetry-preserving first-order superconductor-to-superconductor transition.

Furthermore, the coupling to an applied magnetic field is included in F_{field} , which involves only biquadratic terms. This seems to contradict the discussion in Sec. V, according to which the trilinear terms in Eqs. (37) and (42)–(45) involving the field and two superconducting OPs are possible. Including the impact of the corresponding induced OPs would not make a difference for the understanding of what fundamentally shapes the phase diagram. We think of F as an effective free energy obtained by starting from the free energy including the trilinear couplings and integrating out the induced superconducting OPs. This can be done by minimizing the free energy with respect to these OPs and everywhere replacing them by the solution in terms of primary OPs and magnetic-field components. The expansion of the result in powers of OPs and magnetic-field components can only renormalize terms already present in the free energy since the Landau expansion contains all symmetry-allowed terms up to a given order.

To be specific, we assume $\mathbf{B} \parallel [110]$ for in-plane field orientation in accordance with [11, 14], i.e., an in-plane angle of $\phi = \pi/4$, and parametrize the magnetic field as

$$\mathbf{B} = \begin{pmatrix} B_x \\ B_y \\ B_z \end{pmatrix} = B \begin{pmatrix} \sin \theta \cos \phi \\ \sin \theta \sin \phi \\ \cos \theta \end{pmatrix} = B \begin{pmatrix} \frac{\sin \theta}{\sqrt{2}} \\ \frac{\sin \theta}{\sqrt{2}} \\ \cos \theta \end{pmatrix}. \quad (55)$$

Since the relevant physical processes are expected to happen mostly deep inside the vortex phase, an extra term for field-expulsion is disregarded. The coefficients λ_s^i in F_{field} are understood as effective quantities describing the leading-order limiting effects for the corresponding OPs by the magnetic field.

Regarding the general procedure, we obtain the coefficients of our model from a detailed analysis of the potential landscape and fitting our model to experimental observations, while keeping in mind the insights gained in previous sections. The constraints on the coefficients will mostly be discussed in Sec. VIA, which is concerned with the case $T_N > T_c$. The transition to the case $T_N < T_c$ in subsection VIB will merely involve a change of T_M .

A. Onset of superconductivity inside the magnetic phase: $T_N > T_c$

As a first scenario, we investigate the case of $T_N > T_c$, i.e., we consider phase I to coincide with magnetic dipolar order, while superconductivity sets in at lower temperatures [15]. Experiments suggest a slightly lower transition temperature for Δ_2 compared to Δ_1 [5, 6, 8, 13], hence we set $T_{c1} = 0.34 \text{ K}$ and $T_{c2} = 0.24 \text{ K}$. Moreover, we choose $T_M = 0.54 \text{ K} = T_N$. Note that due to the weak suppression of superconductivity by the magnetic order we obtain $T_c \approx 0.33 \text{ K} \lesssim T_{c1}$ at $\mathbf{B} = 0$.

The calculated phase diagram is shown in Fig. 5 and displays multiple phases, both superconducting and magnetic. There is a magnetic phase setting in via a

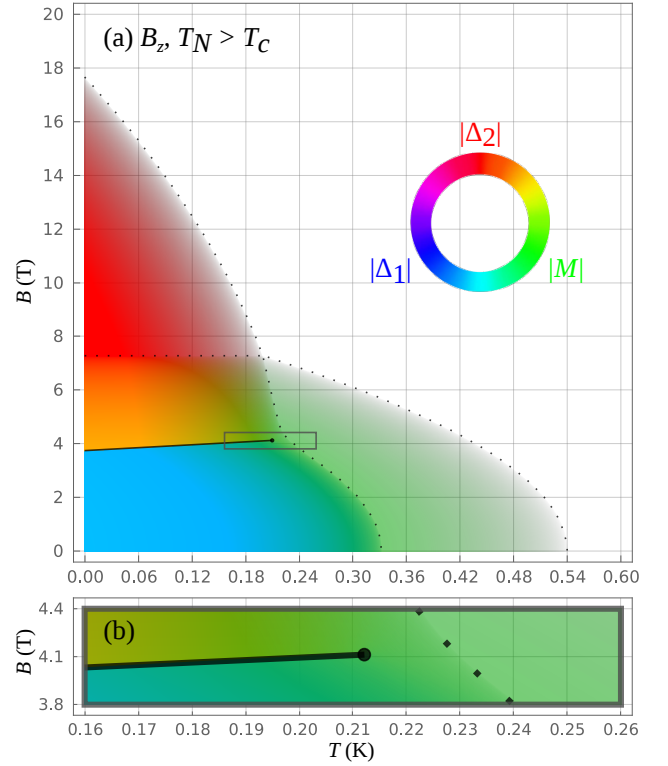


FIG. 5. Phase diagram for out-of-plane magnetic field and $T_N > T_c$ for (a) the full temperature and magnetic-field range and (b) the region close to the end point of the first-order transition. The colors of distinct phases are generated by mixing contributions from $|\Delta_1|$ (blue), $|\Delta_2|$ (red) and $|M|$ (green) into an RGB-triplet and the transparency is determined from the overall OP magnitude. Solid and dotted lines represent first-order and second-order phase transitions, respectively.

second-order transition at T_N , which penetrates both into the high-field and into the low-field phase below the corresponding second-order superconducting transitions. Most intriguingly, our analysis not only shows a first-order transition at $B^* \approx 4 \text{ T}$ between two coexistence phases involving nonzero Δ_1 , Δ_2 , and M but also predicts that the first-order transition line has a critical endpoint. Hence, there is a small crossover region between the endpoint and the second-order superconducting transition line. Figure 5(b) shows a magnification of the corresponding region. At a stronger field of about 7 T, the magnetic OP M and the superconducting OP Δ_1 (of B_{1g+} symmetry) vanish at a second-order transition and only the superconducting OP Δ_2 (of B_{1u+} symmetry) survives. The superconductivity breaks down only at much higher fields.

In Fig. 6, we show the angle-dependent evolution of the phase diagram from out-of-plane to in-plane field orientation. While for a small angle of $\theta = 10^\circ$ between the magnetic field and the z -direction mostly the critical-field values change, already for $\theta = 20^\circ$, the pure Δ_2 phase is completely suppressed. For $\theta = 45^\circ$, also the high-field coexistence phase is almost entirely gone, eventually leav-

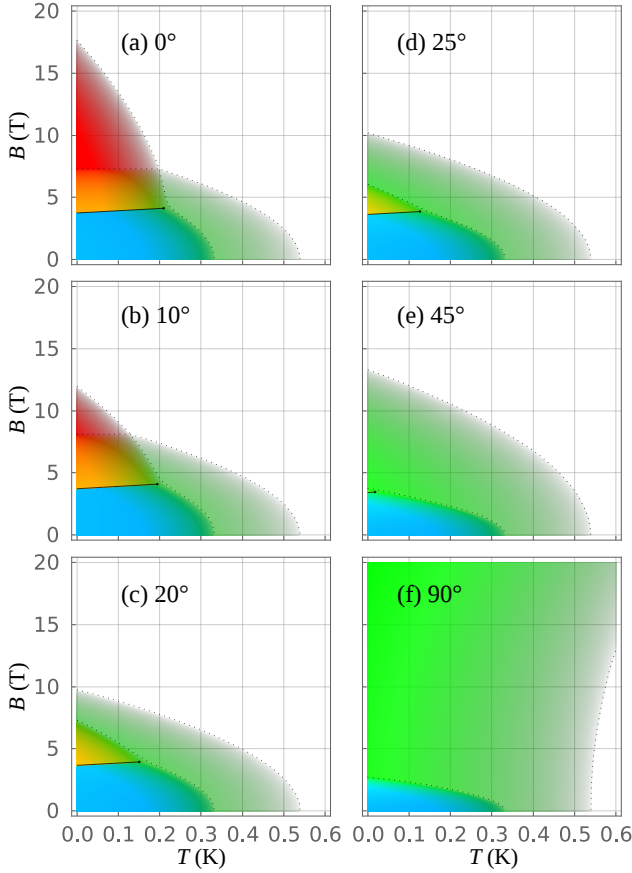


FIG. 6. Phase diagrams in the temperature-magnetic-field plane for $T_N > T_c$ and angles (a) $\theta = 0^\circ$, i.e., $\mathbf{B} \parallel [001]$, (b) $\theta = 10^\circ$, (c) $\theta = 20^\circ$, (d) $\theta = 25^\circ$, (e) $\theta = 45^\circ$, and (f) $\theta = 90^\circ$, i.e., $\mathbf{B} \parallel [110]$, between the magnetic field and the surface normal (z -axis). The color reflects the admixture of distinct OPs as in Fig. 5. Solid and dotted lines represent first-order and second-order phase transitions, respectively.

ing only the low-field coexistence phase and a much enhanced magnetic phase for $\theta = 90^\circ$ (in plane). A strong enhancement of the critical temperature T_0 of phase I in an in-plane magnetic field is indeed observed experimentally [10]. Note that we do not describe the transition between the phases I and II [10–12, 45].

We now take a closer look at the choice of coefficients for our Landau analysis. Without loss of generality, we set the positive fourth-order coefficients to $\beta_1 = \beta_2 = \beta_M = 1$. This amounts to a choice of units for the OPs. The second-order coefficients are expanded in temperature to linear order, see Eqs. (52)–(54). For a magnetic field to be able to induce a transition between the superconducting states, i.e., between the primary OP Δ_1 (B_{1g+}) and the primary OP Δ_2 (B_{1u+}), these states have to be close in energy. Therefore, we set $\alpha'_2 \gtrsim \alpha'_1$, with a slight imbalance to account for the weak tilting of the almost horizontal first-order transition line. Moreover, since the magnetic phase is expected to have a comparatively weak effect we assume $\alpha'_{1,2} > \alpha'_M$.

Next, we investigate the role of coupling terms between OPs. First, it is natural to assume a competition between distinct superconducting orders since they compete for the same electrons and thus γ_{12} should be positive (repulsive). This helps to stabilize the first-order transition. Experimentally, the magnetic phase is slightly suppressed when entering the superconducting phases. For the low-field phase, this can be deduced from the suppression of internal fields B_{int} below T_c seen in NMR measurements [15]. For the high-field phase, the transition line of the magnetic transition deviates from a smooth extrapolation by being tilted towards lower fields. It becomes almost field independent inside the superconducting region [32]. This also indicates a weak suppression. It turns out that $\gamma_{12} \gg \gamma_{2M} \gtrsim \gamma_{1M} > 0$ gives best results. The trilinear coupling term is expected to be weak and we set $0 < |\delta_{12M}| < 1$. However, for the general phenomenology of multicomponent superconducting orders it only needs to be nonzero.

Finally, we discuss the biquadratic coupling terms involving the applied magnetic field. One central experimental observation is the high upper critical field for magnetic field along the z -direction, which far surpasses Pauli limiting. We explained the different contributions to the likely B_{1g+} and B_{1u+} pairing states in Sec. VC, which can be qualitatively modeled by $1 \gg \lambda_1^z > \lambda_M^z \gtrsim \lambda_2^z > 0$.

Angle-resolved measurements of superconductivity in CeRh_2As_2 have shown a strong variation of the upper critical field when tilting the field direction into the xy plane [6]. Note that we assume the in-plane field to be along the $[110]$ direction. In fact, the high-field phases completely vanish for in-plane fields, which we incorporate by choosing $\lambda_2^z \ll \lambda_2^{xy}$. This is not surprising since the in-plane, nearest-neighbor contribution to Δ_2 (B_{1u+}) is exclusively of triplet character, see Table V. This triplet pairing and the triplet contribution from the induced B_{2u+} OP are now suppressed due to the parallel orientation of the applied field and the triplet \mathbf{d} vector, as discussed in section VC. Moreover, our analysis suggests a similar suppression of Δ_1 and Δ_2 for in-plane fields, hence $\lambda_1^{xy} \approx \lambda_2^{xy}$. That is, also the predominantly spin-singlet B_{1g+} low-field pairing faces stronger suppression for in-plane fields, which can again be understood in terms of suppressed primary and induced (B_{2g+}) spin-triplet contributions. Besides, in sections VA and VB, we concluded that induced superconducting OPs can help to stabilize superconductivity for fields along the z -direction but not for fields within the basal plane [46].

Apart from the positive coefficients mentioned above, we introduce a small but negative coefficient $\lambda_M^{xy} < 0$ for the coupling of the magnetic OP to an in-plane field since such a field was experimentally observed to stabilize the T_0 phase—recall that we identify this phase with AFM order. In this context, the field-induced mixing of the Γ_6 excited doublet with the $\Gamma_7^{(1)}$ ground-state doublet has been discussed, see Fig. 1, leading to the stabilization of

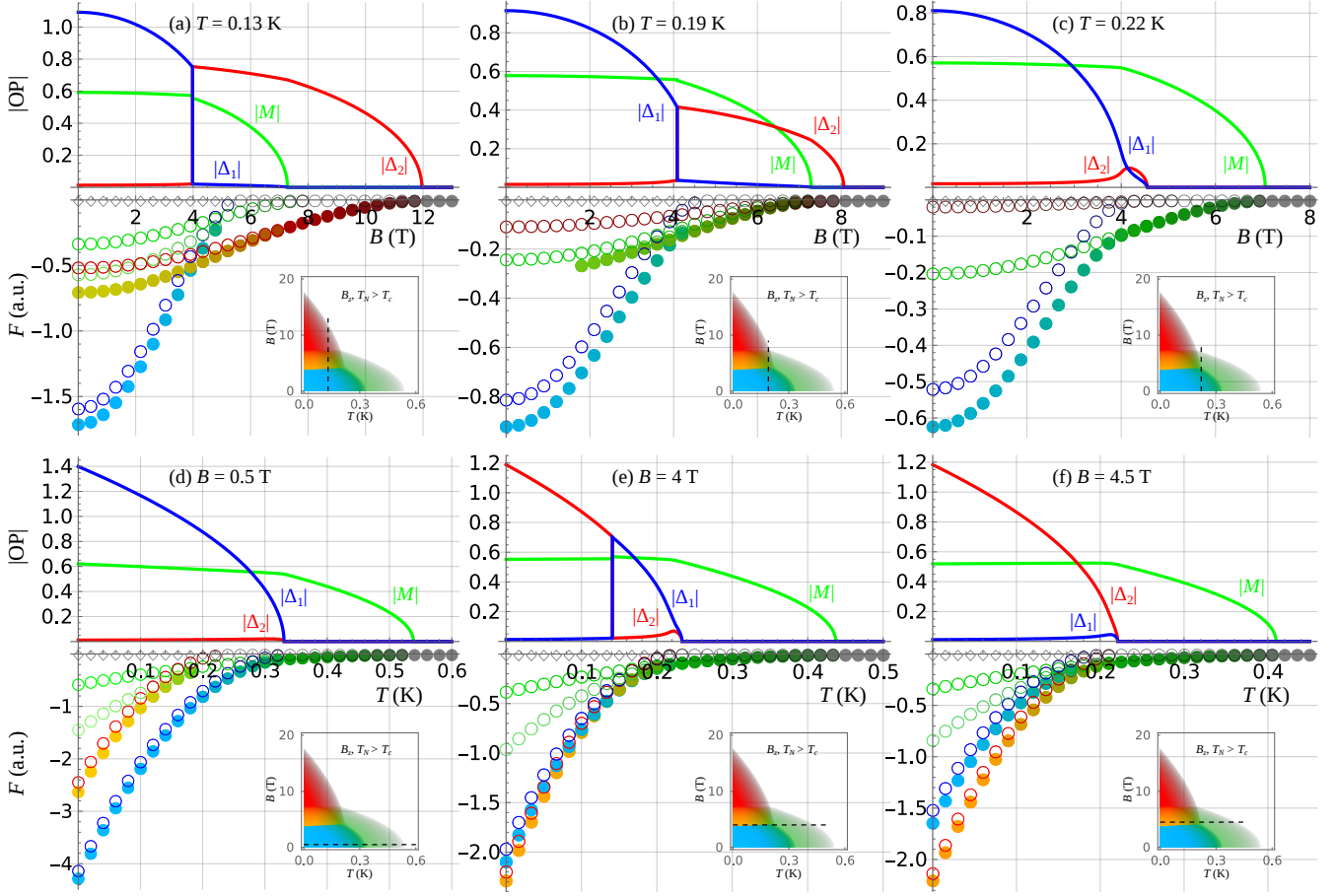


FIG. 7. Order-parameter amplitudes and free energies at stationary points along various cuts through the phase diagram for $T_N > T_c$ and magnetic field along the z -direction. The cuts in the upper row are at a constant temperature of (a) $T = 0.13$ K, (b) $T = 0.19$ K, and (c) $T = 0.22$ K. The cuts in the lower row are at a constant magnetic field of (d) $B = 0.5$ T, (e) $B = 4$ T, and (f) $B = 4.5$ T. The cuts are also indicated in the insets. The symbol \bullet denotes minima of the free energy, while saddle points and maxima are denoted by \circ and \diamond , respectively. The color of the symbols reflects the admixture of distinct OPs, whose amplitudes are given in the corresponding upper part of the panels.

in-plane AFM order by field-induced dipole-quadrupole coupling [45]. This results in a transition between multipolar phases I and II. This transition is not captured by our Landau functional, which does not contain higher multipolar OPs since our main focus lies on the superconducting states. Therefore, we effectively approximate the stabilization by an attractive coupling $\lambda_M^{xy} < 0$.

The complete set of coefficients is the following: $\alpha'_1 = 12$, $\alpha'_2 = 13$, $\alpha'_M = 2.8$, $\beta_1 = \beta_2 = \beta_M = 1$, $\gamma_{12} = 12$, $\gamma_{1M} = 0.38$, $\gamma_{2M} = 0.44$, $\delta_{12M} = -0.55$, $\lambda_1^z = 0.08$, $\lambda_2^z = 0.01$, $\lambda_M^z = 0.018$, $\lambda_1^{xy} = 0.5$, $\lambda_2^{xy} = 0.4$, $\lambda_M^{xy} = -0.001$.

In Fig. 7, we show plots of the OP amplitudes and free energy for various cuts through the phase diagram, tuning either the magnetic field or the temperature. In panels (a) and (b), we observe a clear jump of $|\Delta_1|$ and $|\Delta_2|$ when crossing the first-order transition at $B^* \approx 4$ T, which is accompanied by a discontinuous change of slope of the lowest minimum of the free energy. However, all three OPs remain nonzero up to the second-order transi-

tion to a pure Δ_2 phase at higher fields. At a slightly higher temperature of $T = 0.22$ K, panel (c), we observe that the first-order transition line is replaced by a smooth crossover. An experimental observation of such a crossover region would be a direct verification of our proposal of a symmetry-preserving first-order transition between two multicomponent superconducting phases. In panels (d)–(f), the aforementioned suppression of the magnetic OP when entering the superconducting region can be observed. Panel (e) once again shows a jump in OP amplitudes when crossing the first-order transition line, which is not completely horizontal.

B. Onset of magnetism below the superconducting transition: $T_N < T_c$

In this subsection, we discuss the scenario of $T_N < T_c$ based on NMR and NQR measurements [8, 13]. The main idea here is to assume that the coefficient α_M

controlling the dynamical magnetic order depends on the experimental timescale [15], as discussed in Sec. IV, whereas the superconducting properties do not. We effectively achieve this by changing a single parameter, namely the magnetic critical temperature T_M from $T_M = 0.54$ K to $T_M = 0.32$ K, which is slightly below $T_c = T_{c1} = 0.34$ K but above $T_{c2} = 0.24$ K.

The overall phase diagram now changes dramatically. In particular, for out-of-plane fields, no stable purely magnetic phase is realized, as is shown in Fig. 8. The first transition which occurs for decreasing temperature at $B = 0$ is a second-order superconducting transition at T_c into a pure Δ_1 (B_{1g+}) phase, followed by another second-order transition at T_N , where time-reversal symmetry breaks. Below T_N , the OPs Δ_1 , Δ_2 , and M coexist. Note that at $\mathbf{B} = 0$ the actual Néel temperature T_N resulting from our calculations lies closer to T_{c2} than to T_M , i.e., $T_M \neq T_N \gtrsim 0.24$ K = T_{c2} . This can be understood in terms of the suppression of magnetism by the superconducting phase Δ_1 , as well as the trilinear coupling between the three OPs which in return facilitates a stabilization close to the onset of Δ_2 . Furthermore, the almost horizontal first-order transition now happens either between the pure Δ_1 -phase or the low-field coexistence-phase and a pure Δ_2 -phase at higher field. A high-field coexistence phase is not found for B along the z -direction. Note that the occurrence of an end point and crossover region are not possible in this case, since the first-order transition involves symmetry breaking.

If the applied field is tilted away from the z -direction the high-field phase vanishes between angles $\theta = 10^\circ$ and $\theta = 20^\circ$. Moreover, a narrow region of purely magnetic OP sets in at $\theta = 10^\circ$ and is clearly visible at $\theta = 20^\circ$. This region is marked by arrows in Figs. 9 (b) and (c), respectively. Therefore, the absence of symmetry breaking again enables the appearance of a small crossover region between two coexistence phases and an endpoint of the first-order transition line. Like for $T_N > T_c$, at an angle of 20° , the pure Δ_2 state has disappeared. This evolution continues for larger angles θ , until for $\theta = 90^\circ$ the magnetic OP is stable over a broad region of the phase diagram. However, in contrast to $T_N > T_c$, we still find a finite region of pure Δ_1 superconducting order since $T_N < T_c$ remains true for all angles. We note an interesting observation for $\theta = 90^\circ$: the magnetic and superconducting transitions almost exactly coincide at $B = 0.8$ T, the field strength at which recent NMR measurements with $\mathbf{B} \parallel [110]$ were performed [14]. This can be seen in Fig. 10 and could be an alternative explanation for the nearly simultaneous onset of both line-width broadening and superconductivity, as opposed to the case of magnetic field along the z -direction [8, 13].

It is quite remarkable that both topologies of the phase diagram for out-of-plane magnetic field, i.e., $T_N > T_c$ and $T_N < T_c$, can be obtained by tuning a single parameter. We find that respecting a broad range of known experimental features for both scenarios and for variable field

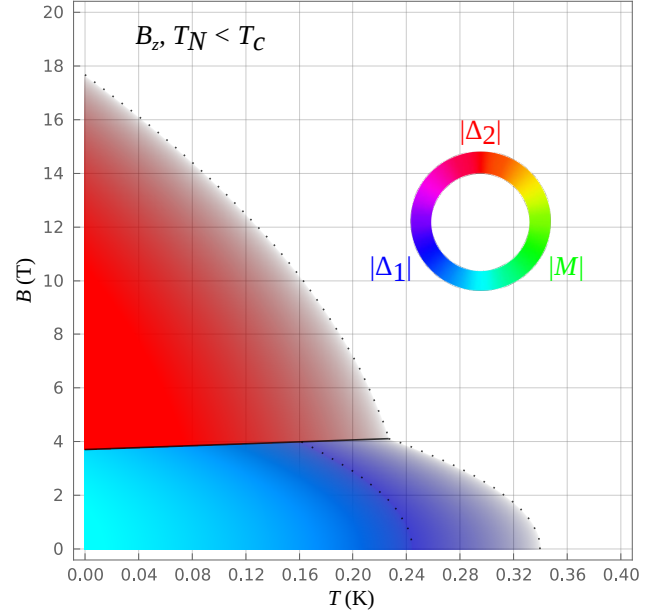


FIG. 8. Phase diagram in the temperature-magnetic-field plane for out-of-plane magnetic field and $T_N < T_c$. The colors of distinct phases are generated by mixing contributions from $|\Delta_1|$ (blue), $|\Delta_2|$ (red) and $|M|$ (green) into an RGB-triplet and the transparency is determined from the overall OP magnitude. Solid and dotted lines represent first-order and second-order phase transitions, respectively.

angle imposes strong constraints on the choice of parameters. For example, a weaker repulsion γ_{12} between the two primary superconducting OPs would lead to the penetration of magnetic order into the high-field phase also for $T_N < T_c$ and thus a high-field coexistence phase for magnetic field along the z -direction, which is not suggested experimentally [8]. Given the present parameter set, the constraint on γ_{12} is less relevant for $T_N > T_c$, where also smaller γ_{12} would suffice. However, a scenario of a very narrow high-field coexistence region for $T_N < T_c$ would also be in agreement with available NMR data [8].

Figure 11 shows the evolution of the OP amplitudes and free energy for various cuts through the phase diagram. In panel (a) for constant $T = 0.13$ K, a large jump of all three OPs at the first-order transition can be seen. The high-field phase here only contains a nonzero OP Δ_2 . Panels (b) and (c) for higher temperatures instead show a disappearance of the magnetic OP and therefore also of Δ_2 before reaching the first-order line. Hence, this first-order transition separates pure Δ_1 and Δ_2 phases, i.e., phases of different symmetry. Therefore, the first-order transition line cannot end in a critical point, unlike for $T_N > T_c$.

Due to the stabilization of magnetic order at lower temperatures and the competition with the pre-existing OP Δ_1 , the magnetic order realizes much smaller amplitudes compared to $T_N > T_c$. Therefore, Δ_2 is extremely small in the coexistence phase. At the first-order transition ($B^* \approx 4$ T), the first derivative of the free en-

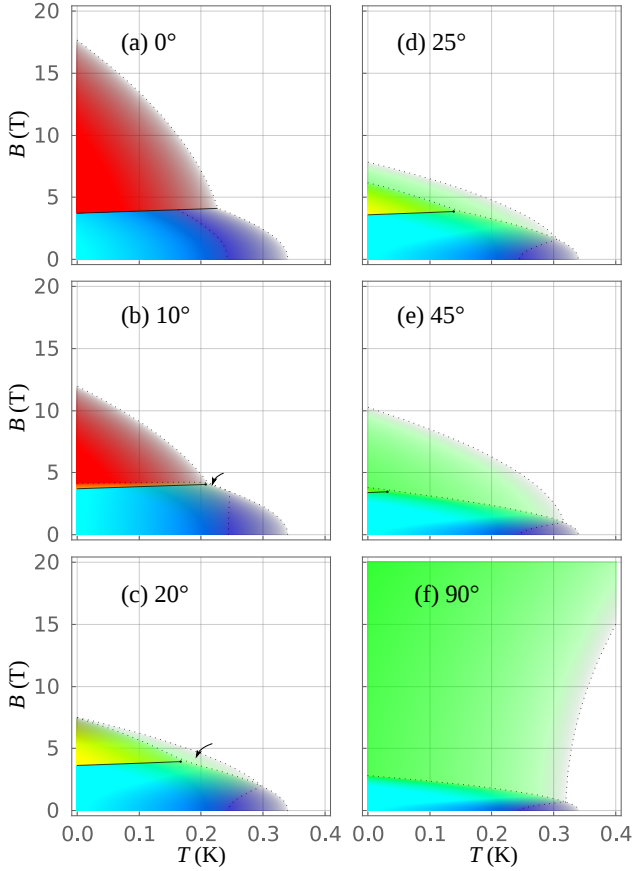


FIG. 9. Phase diagrams in the temperature-magnetic-field plane for $T_N < T_c$ and angles (a) $\theta = 0^\circ$, i.e., $\mathbf{B} \parallel [001]$, (b) $\theta = 10^\circ$, (c) $\theta = 20^\circ$, (d) $\theta = 25^\circ$, (e) $\theta = 45^\circ$, and (f) $\theta = 90^\circ$, i.e., $\mathbf{B} \parallel [110]$, between the magnetic field and the surface normal (z -axis). The color reflects the admixture of distinct OPs as in Fig. 8. Solid and dotted lines represent first-order and second-order phase transitions, respectively.

ergy again jumps when one minimum becomes disfavored with respect to another already existing minimum. For $T_N < T_c$, most of the minima are accompanied by almost degenerate saddle points, denoted by open circles in Fig. 11. Panel (d) shows the second-order transition into the Δ_1 phase and subsequently into the low-field coexistence phase with magnetic order. Like for the case of $T_N > T_c$, a discontinuity of $|\Delta_1|$ and $|\Delta_2|$ occurs when the cut intersects the slightly tilted first-order line in panel (e). Panel (f) only shows the mean-field onset of the high-field order Δ_2 .

VII. THERMODYNAMICS

With the Landau free energy at hand, we can estimate experimentally relevant derivatives, e.g., thermodynamic quantities such as the specific heat or the susceptibility. In this section, we will focus on the case of $T_N > T_c$ and a magnetic field oriented along the z -direction. Note

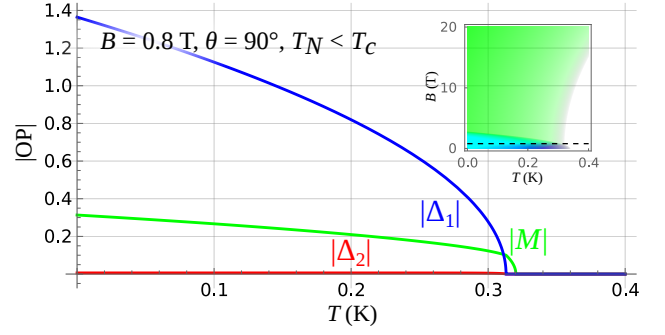


FIG. 10. Order-parameter amplitudes for in-plane field ($\mathbf{B} \parallel [110]$) and $T_N < T_c$ at constant field $B = 0.8$ T. Here, Δ_1 and M , and therefore also Δ_2 , order at closely proximate temperatures.

that Landau theory, which involves an expansion in small order parameters, is not expected to give quantitatively accurate results for temperatures far below T_c and T_N .

Furthermore, our Landau functional does not contain the energy cost of the flux expulsion and thus does not account for the transition from the Meißner to the Shubnikov phase. Note that the corresponding lower critical field is much smaller than the characteristic field scale of the first-order superconductor-to-superconductor transition. Therefore, when calculating derivatives with respect to the magnetic field, we miss the contribution from flux expulsion. Nevertheless, we find qualitative agreement with recent experimental data for the uniform, isothermal susceptibility

$$\chi_T = - \left(\frac{\partial^2 F}{\partial B^2} \right)_T. \quad (56)$$

In Fig. 12, χ_T is plotted as a function of magnetic field for three temperatures. For $T = 0.13$ K and $T = 0.19$ K, the path in the phase diagram intersects the first-order transition at $B^* \approx 4$ T, indicated by a clear jump, followed by a smaller jump when the pure high-field superconducting state is reached at around $B_0 \approx 7$ T. Moreover, we observe a steeper slope of χ_T vs. B below B^* than above. These observations are compatible with, for instance, the data shown in Fig. S5 of Ref. [32]. At $T = 0.22$ K, we see that near B^* the susceptibility smoothly changes with the field and no phase transition is observable, which is a hallmark of the underlying crossover region. Such behavior might be difficult to distinguish from an experimentally broadened phase transition and could be hidden in previously reported data. The smooth behavior of χ_T continues until the upper critical field is reached, indicated by a small kink near $B_{c2} \approx 4.5$ T.

The specific heat at constant magnetic field is given by

$$C_B = -T \left(\frac{\partial^2 F}{\partial T^2} \right)_B. \quad (57)$$

In Fig. 13, we plot C_B as a function of temperature for three values of the magnetic field. In all cases, a small

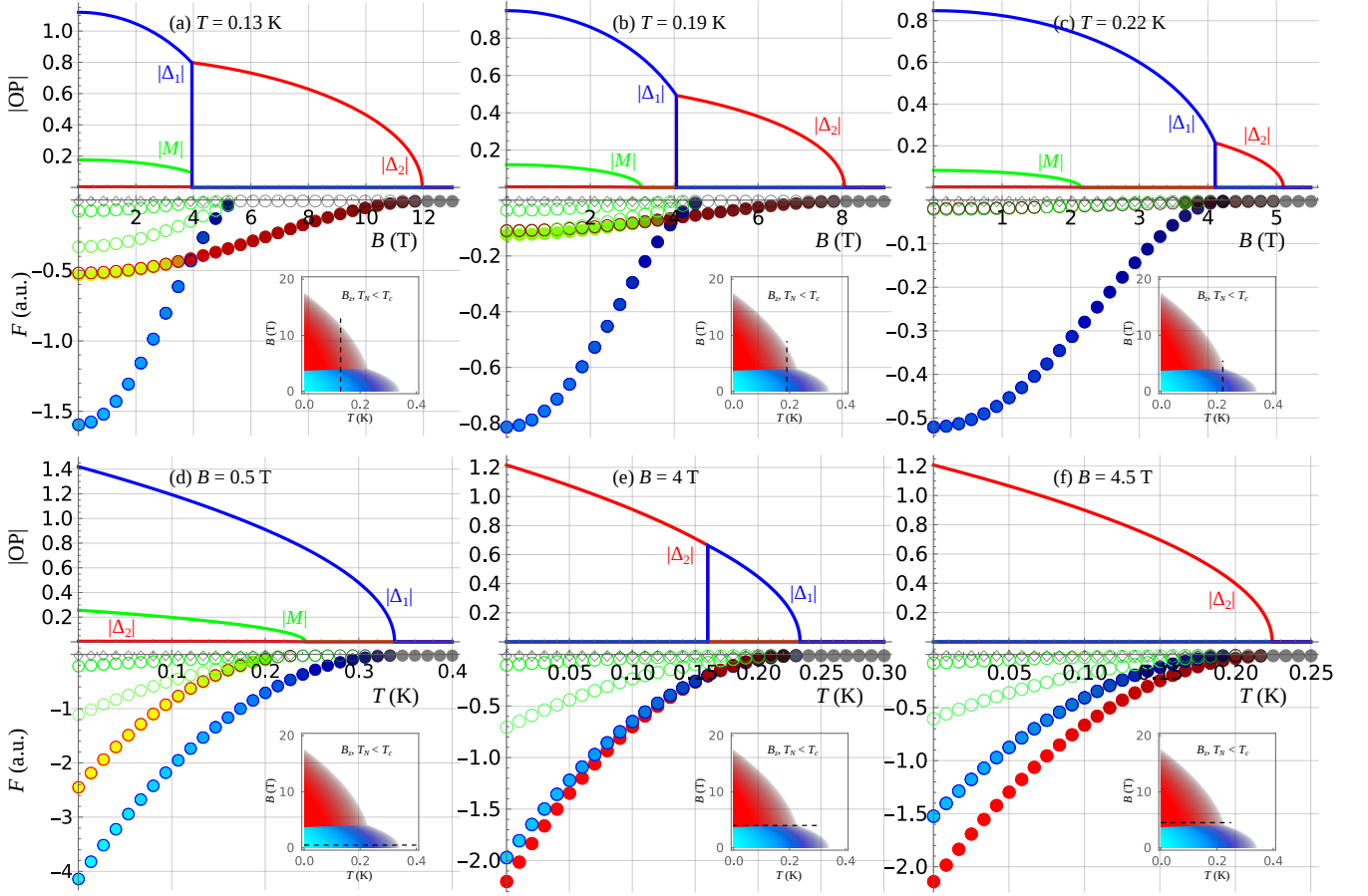


FIG. 11. Order-parameter amplitudes and free energies at stationary points along various cuts through the phase diagram for $T_N < T_c$ and magnetic field along the z -direction. The cuts in the upper row are at a constant temperature of (a) $T = 0.13$ K, (b) $T = 0.19$ K, and (c) $T = 0.22$ K. The cuts in the lower row are at a constant magnetic field of (d) $B = 0.5$ T, (e) $B = 4$ T, and (f) $B = 4.5$ T. The cuts are also indicated in the insets. The symbol \bullet denotes minima of the free energy, while saddle points and maxima are denoted by \circ and \diamond , respectively. The color of the symbols reflects the admixture of distinct OPs, whose amplitudes are given in the corresponding upper part of the panels.

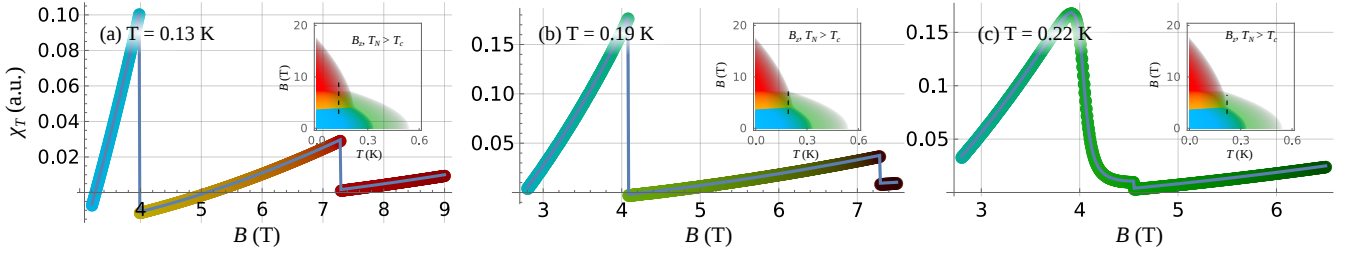


FIG. 12. Isothermal susceptibility χ_T for $T_N > T_c$ and $\mathbf{B} \parallel [001]$ as a function of magnetic field at (a) $T = 0.13$ K, (b) $T = 0.19$ K, and (c) $T = 0.22$ K. The corresponding cuts through the phase diagram are indicated in the insets. In panels (a) and (b), χ_T shows a jump at the first-order transition near $B^* \approx 4$ T, as well as at the second-order transition near $B_0 \approx 7$ T. Panel (c) shows a smooth transition in the crossover region near B^* and a kink at $B_{c2} \approx 4.5$ T.

jump is visible at the magnetic transition at T_N and a larger jump at T_c . Both transitions are of second order. Panel (b) for $B = 4$ T additionally shows a small kink at $T^* \approx 0.14$ K, the intersection with the first-order superconductor-to-superconductor transition, similar to Fig. 3(a) of Ref. [32]. Note that the cut in panel (b) but

also the one in panel (c) pass quite close to the predicted critical end point at about 0.21 K, see also Fig. 5. We interpret the pronounced maximum in C_B as a fingerprint of the critical end point. In addition, we observe a small upturn in C_B immediately below T_c in panel (b). Its extent is primarily determined by and increases with

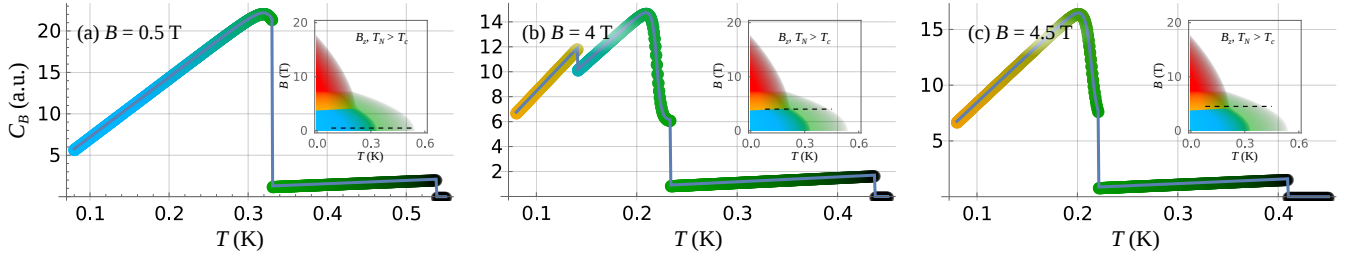


FIG. 13. Specific heat C_B as a function of temperature for $T_N > T_c$ and magnetic field (a) $B = 0.5$ T, (b) $B = 4$ T, and (c) $B = 4.5$ T along the z -direction. The cuts are indicated in the insets. In all panels, a small jump is visible at T_N , which at lower temperature is followed by a large jump at T_c . Both transitions are of second order. Panel (b) additionally shows a small kink at T^* when intersecting the first-order superconductor-to-superconductor transition.

the trilinear coupling coefficient δ_{12M} . Intriguingly, this kink-like anomaly has actually been observed experimentally, see Figs. 1 and 2 of Ref. [47]. The authors interpret it as an additional first-order phase transition within the superconducting state. However, the anomaly was not observed in the specific heat below $B \approx 3$ T and above $B \approx 5$ T [47]. This behavior agrees with our prediction that the anomaly should only appear in the vicinity of the critical end point.

Our calculations further indicate that the experimental signatures when crossing the superconductor-to-superconductor transition are indeed consistent with a first-order transition. This helps to resolve the recently raised concern regarding the order of this transition [32].

VIII. SUMMARY AND CONCLUSIONS

Materials lacking inversion symmetry, i.e., noncentrosymmetric materials, often display unique magnetic and magnetoelectric behavior and potentially support topological superconductivity [48]. Lately, significant interest has emerged in crystal structures that break inversion symmetry locally but not globally. Superconductivity in such locally noncentrosymmetric materials can exhibit phenomena that would not usually be expected in centrosymmetric systems [1–4].

One important class of locally noncentrosymmetric crystal structures consists of layered materials characterized by inversion centers between the layers but not within them. The tetragonal heavy-fermion superconductor CeRh_2As_2 is a nonsymmorphic representative of this class, in which two layers per unit cell form two Ce sublattices. Another example is the family of superconductors based on the also nonsymmorphic structure $\text{BiS}_{2-n}\text{Se}_n$, including $\text{LaO}_{0.5}\text{Fe}_{0.5}\text{BiSe}_2$ [4, 49]. Both CeRh_2As_2 and $\text{LaO}_{0.5}\text{Fe}_{0.5}\text{BiSe}_2$ have point group D_{4h} and space group $P4/nmm$. The quasitetragonal cuprate $\text{Bi}_2\text{Sr}_2\text{CaCu}_2\text{O}_{8+\delta}$ [4, 50–53] is a symmorphic example with point group D_{2h} and space group $Bbmb$.

In this work, we have addressed the open question of probable symmetries of the ordered phases in the rich temperature-magnetic-field phase diagram of CeRh_2As_2 ,

taking into account most recent experimental data from NQR [31], NMR [8, 14], μSR [15], and thermodynamic measurements [5, 6, 10, 11, 32]. Within a theoretical framework based on symmetry analysis as well as Bogoliubov–de Gennes and Landau methods, we have made concrete predictions regarding the symmetry of superconducting and magnetic ordering phenomena, as well as their interaction.

The resulting superconducting pairing is predominantly of sublattice-even spin-singlet type of B_{1g} symmetry at low fields, whereas the high-field order is dominated by sublattice-even spin-triple pairing of B_{1u} symmetry. In agreement with [9, 17, 25, 26], we argue that superconducting OPs belonging to B irreps are preferred over OPs belonging to A irreps because A_{1g} and A_{2u} orders are suppressed by the expected strongly repulsive Hubbard repulsion U in this heavy-fermion compound.

An important perspective resulting from our calculations is that of not only multiphase but also multicomponent superconductivity in CeRh_2As_2 . Here, we observe the generic coexistence of the primary low-field superconducting OP of B_{1g} symmetry and the primary high-field superconducting OP of B_{1u} symmetry in multiple regions of the phase diagram, enabled by the trilinear coupling term between the superconducting orders and the AFM phase of A_{1u} symmetry. Moreover, this scenario predicts the characteristic first-order superconductor-to-superconductor transition to preserve symmetry. In the low-field and high-field coexistence phases, the same superconducting and magnetic OPs are realized, albeit with different amplitudes. One manifestation of this phenomenology is the observed critical end point of the first-order line when approaching the second-order superconducting transition, followed by a crossover region. We note that the applied magnetic field induces additional superconducting OPs, described by trilinear terms involving two superconducting OPs and the magnetic field.

Our approach consistently reproduces experimental results for both $T_N > T_c$ and $T_N < T_c$, i.e., for both orderings of the zero-field critical temperatures of magnetic order and superconductivity. Phase diagrams of both types have been reported based on different experimental probes [13–15], perhaps due to the interplay of

dynamical magnetic order and experimental timescales [15]. Notably, it is sufficient to assume a single parameter, namely the critical temperature T_M , to depend on the experimental probe. Our approach also correctly describes the phase diagrams for general angles θ between the magnetic field and the surface normal.

One might question whether we are “fitting an elephant” since the Landau functional contains a large number of parameters. This is not so. Reproducing the three-dimensional phase diagrams in the space of temperature, out-of-plane field, and in-plane field for both $T_N > T_c$ and $T_N < T_c$ strongly constrains the parameters. The fact that this is possible at all thus suggests that it is based on a valid physical picture.

Our work answers open questions regarding the order of the superconductor-to-superconductor phase transitions, as well as questions regarding the symmetry of competing orders, including a refined picture of their interplay. In particular, our proposal of multicomponent superconductivity and its implications redirect research on CeRh_2As_2 away from the paradigm of single-OP phases. Moreover, a symmetry preserving first-order superconductor-to-superconductor transition represents a novel discovery in the context of unconventional superconductivity and CeRh_2As_2 is a promising candidate

to exhibit this phenomenon. Our calculations of thermodynamic observables suggest that signatures of such a transition—involving a critical end point and a crossover regime—may in fact be identified in available experimental data. At a more general level, our findings show the importance of symmetry-allowed but nontrivial couplings between superconducting and magnetic OPs, represented by trilinear terms in the Landau functional. In the present case, they lead to a strong connection between local inversion-symmetry breaking, even-parity and odd-parity superconductivity, as well as magnetic order.

ACKNOWLEDGMENTS

The authors wish to thank M. Brando, P. M. R. Brydon, C. Geibel, E. Hassinger, P. Khanenko, S. Khim, J. F. Landaeta, B. Nally, M. Pfeiffer, A. Ramires, B. Schmidt, A. L. Szabó, and K. Semeniuk for useful discussions and sharing their data. Financial support by Deutsche Forschungsgemeinschaft, in part through Collaborative Research Center SFB 1143, project A04, project id 247310070, and Würzburg-Dresden Cluster of Excellence ct.qmat, EXC 2147, project id 390858490, is gratefully acknowledged.

-
- [1] M. H. Fischer, F. Loder, and M. Sigrist, Superconductivity and local noncentrosymmetry in crystal lattices, *Phys. Rev. B* **84**, 184533 (2011).
 - [2] D. Maruyama, M. Sigrist, and Y. Yanase, Locally non-centrosymmetric superconductivity in multilayer systems, *J. Phys. Soc. Jpn.* **81**, 034702 (2012).
 - [3] M. Sigrist, D. F. Agterberg, M. H. Fischer, J. Goryo, F. Loder, S.-H. Rhim, D. Maruyama, Y. Yanase, T. Yoshida, and S. J. Youn, Superconductors with staggered non-centrosymmetry, *J. Phys. Soc. Jpn.* **83**, 061014 (2014).
 - [4] M. H. Fischer, M. Sigrist, D. F. Agterberg, and Y. Yanase, Superconductivity and Local Inversion-Symmetry Breaking, *Annu. Rev. Condens. Matter Phys.* **14**, 040521 (2023).
 - [5] S. Khim, J. F. Landaeta, J. Banda, N. Bannor, M. Brando, P. M. R. Brydon, D. Hafner, R. Kuchler, R. Cardoso-Gil, U. Stockert, A. P. Mackenzie, D. F. Agterberg, C. Geibel, and E. Hassinger, Field-induced transition within the superconducting state of CeRh_2As_2 , *Science* **373**, 1012 (2021).
 - [6] J. F. Landaeta, P. Khanenko, D. C. Cavanagh, C. Geibel, S. Khim, S. Mishra, I. Sheikin, P. M. R. Brydon, D. F. Agterberg, M. Brando, and E. Hassinger, Field-Angle Dependence Reveals Odd-Parity Superconductivity in CeRh_2As_2 , *Phys. Rev. X* **12**, 031001 (2022).
 - [7] D. C. Cavanagh, T. Shishidou, M. Weinert, P. M. R. Brydon, and D. F. Agterberg, Nonsymmorphic symmetry and field-driven odd-parity pairing in CeRh_2As_2 , *Phys. Rev. B* **105**, L020505 (2022).
 - [8] S. Ogata, S. Kitagawa, K. Kinjo, K. Ishida, M. Brando, E. Hassinger, C. Geibel, and S. Khim, Parity Transition of Spin-Singlet Superconductivity Using Sublattice Degrees of Freedom, *Phys. Rev. Lett.* **130**, 166001 (2023).
 - [9] B. K. Nally and P. M. R. Brydon, Phase diagram of strongly-coupled Rashba systems, *New J. Phys.* **26**, 093015 (2024).
 - [10] D. Hafner, P. Khanenko, E.-O. Eljaouhari, R. Kuchler, J. Banda, N. Bannor, T. Lühmann, J. F. Landaeta, S. Mishra, I. Sheikin, E. Hassinger, S. Khim, C. Geibel, G. Zwicknagl, and M. Brando, Possible Quadrupole Density Wave in the Superconducting Kondo Lattice CeRh_2As_2 , *Phys. Rev. X* **12**, 011023 (2022).
 - [11] P. Khanenko, D. Hafner, K. Semeniuk, J. Banda, T. Lühmann, F. Bärthel, T. Kotte, J. Wosnitza, G. Zwicknagl, C. Geibel, J. F. Landaeta, S. Khim, E. Hassinger, and M. Brando, Origin of the non-Fermi-liquid behavior in CeRh_2As_2 , *Phys. Rev. B* **111**, 045162 (2025).
 - [12] S. Mishra, Y. Liu, E. D. Bauer, F. Ronning, and S. M. Thomas, Anisotropic magnetotransport properties of the heavy-fermion superconductor CeRh_2As_2 , *Phys. Rev. B* **106**, L140502 (2022).
 - [13] M. Kibune, S. Kitagawa, K. Kinjo, S. Ogata, M. Manago, T. Taniguchi, K. Ishida, M. Brando, E. Hassinger, H. Rosner, C. Geibel, and S. Khim, Observation of Antiferromagnetic Order as Odd-Parity Multipoles inside the Superconducting Phase in CeRh_2As_2 , *Phys. Rev. Lett.* **128**, 057002 (2022).
 - [14] S. Ogata, S. Kitagawa, K. Kinjo, K. Ishida, M. Brando, E. Hassinger, C. Geibel, and S. Khim, Appearance of c-axis magnetic moment in odd-parity antiferromagnetic state in CeRh_2As_2 revealed by ^{75}As -NMR, *Phys. Rev. B* **110**, 214509 (2024).

- [15] S. Khim, O. Stockert, M. Brando, C. Geibel, C. Baines, T. J. Hicken, H. Luetkens, D. Das, T. Shiroka, Z. Guguchia, and R. Scheuermann, Coexistence of local magnetism and superconductivity in the heavy-fermion CeRh_2As_2 revealed by μSR studies, [arXiv:2406.16575 \(2024\)](#).
- [16] C. Timm and A. Bhattacharya, Symmetry, nodal structure, and Bogoliubov Fermi surfaces for nonlocal pairing, *Phys. Rev. B* **104**, 094529 (2021).
- [17] A. Amin, H. Wu, T. Shishidou, and D. F. Agterberg, Kramers' degenerate magnetism and superconductivity, *Phys. Rev. B* **109**, 024502 (2024).
- [18] G. Zwignagl, Quasi-particles in heavy fermion systems, *Adv. Phys.* **41**, 203 (1992).
- [19] G. Zwignagl, The utility of band theory in strongly correlated electron systems, *Rep. Progr. Phys.* **79**, 124501 (2016).
- [20] K. Nogaki, A. Daido, J. Ishizuka, and Y. Yanase, Topological crystalline superconductivity in locally noncentrosymmetric CeRh_2As_2 , *Phys. Rev. Res.* **3**, L032071 (2021).
- [21] G. Katzer, Character Tables for Point Groups used in Chemistry, http://gernot-katzers-spice-pages.com/character_tables/.
- [22] Since the matrix h_5 is diagonal in the sublattice index the basis function contains sine and cosine functions of integer multiples of k_x, k_y, k_z . The functions multiplying the off-diagonal matrices h_1 and h_2 have to describe hopping over half-integer separations and therefore contain sine and cosine functions of half-integer multiples of k_x, k_y, k_z . See also Ref. [17].
- [23] P. A. Frigeri, D. F. Agterberg, A. Koga, and M. Sigrist, Superconductivity without Inversion Symmetry: MnSi versus CePt_3Si , *Phys. Rev. Lett.* **92**, 097001 (2004).
- [24] If CeRh_2As_2 for some reason had π junctions the general form of the results would remain the same, only the partner irreps would be interchanged.
- [25] C. Lee, D. F. Agterberg, and P. M. R. Brydon, Unified picture of superconductivity and magnetism in CeRh_2As_2 , [arXiv:2407.00536 \(2024\)](#).
- [26] K. Nogaki and Y. Yanase, Even-odd parity transition in strongly correlated locally noncentrosymmetric superconductors: Application to CeRh_2As_2 , *Phys. Rev. B* **106**, L100504 (2022).
- [27] Except for the double layers, these constraints rely on longer-range dipole fields. The field at the As(1) sites from breaking these constraints may be too weak to observe.
- [28] The moments in even-numbered and odd-numbered double layers could, in principle, be constrained by measuring the magnetic field at the Rh(1) sites.
- [29] A. L. Szabó and A. Ramires, Superconductivity-induced improper orders in nonsymmorphic systems, *Phys. Rev. B* **110**, L180503 (2024).
- [30] Conversely, A_{2g-} , E_{g-} , and E_{u-} would lead to nonzero fields at all As sites, B_{2u-} to nonzero field only at As(1) sites, and all other TR-odd irreps to vanishing field at all As sites.
- [31] S. Kitagawa, M. Kibune, K. Kinjo, M. Manago, T. Taniguchi, K. Ishida, M. Brando, E. Hassinger, C. Geibel, and S. Khim, Two-Dimensional XY-Type Magnetic Properties of Locally Noncentrosymmetric Superconductor CeRh_2As_2 , *J. Phys. Soc. Jpn.* **91**, 043702 (2022).
- [32] P. Khanenko, J. F. Landaeta, S. Ruet, T. Lühmann, K. Semeniuk, M. Pelly, A. W. Rost, G. Chajewski, D. Kaczorowski, C. Geibel, S. Khim, E. Hassinger, and M. Brando, The phase diagram of CeRh_2As_2 for out-of-plane magnetic field, [arXiv:2504.15112 \(2025\)](#).
- [33] M. Sigrist and K. Ueda, Phenomenological theory of unconventional superconductivity, *Rev. Mod. Phys.* **63**, 239 (1991).
- [34] P. M. R. Brydon, D. F. Agterberg, H. Menke, and C. Timm, Bogoliubov Fermi surfaces: General theory, magnetic order, and topology, *Phys. Rev. B* **98**, 224509 (2018).
- [35] K. Machida, Violation of Pauli-Clogston limit in the heavy-fermion superconductor CeRh_2As_2 : Duality of itinerant and localized 4f electrons, *Phys. Rev. B* **106**, 184509 (2022).
- [36] The convention for the components is the same as for the doublets (σ_x, σ_y) and (B_x, B_y) in the case of E_g and the same multiplied by an A_{1u} basis function in the case of E_u . With this choice, the expressions for g and u irreps are the same.
- [37] A. L. Szabó, M. H. Fischer, and M. Sigrist, Effects of nucleation at a first-order transition between two superconducting phases: Application to CeRh_2As_2 , *Phys. Rev. Res.* **6**, 023080 (2024).
- [38] E. G. Schertenleib, M. H. Fischer, and M. Sigrist, Unusual H - T phase diagram of CeRh_2As_2 : The role of staggered noncentrosymmetry, *Phys. Rev. Res.* **3**, 023179 (2021).
- [39] B. S. Chandrasekhar, A note on the maximum critical field of high-field superconductors, *Appl. Phys. Lett.* **1**, 7 (1962).
- [40] A. M. Clogston, Upper Limit for the Critical Field in Hard Superconductors, *Phys. Rev. Lett.* **9**, 266 (1962).
- [41] N. R. Werthamer, E. Helfand, and P. C. Hohenberg, Temperature and purity dependence of the superconducting critical field, H_{c2} . III. Electron spin and spin-orbit effects, *Phys. Rev.* **147**, 295 (1966).
- [42] P. Fulde and R. A. Ferrell, Superconductivity in a Strong Spin-Exchange Field, *Phys. Rev.* **135**, A550 (1964).
- [43] A. I. Larkin and Y. N. Ovchinnikov, Nonuniform state of superconductors, *Sov. Phys. JETP* **20**, 762 (1965).
- [44] J. R. Schrieffer, *Theory of Superconductivity* (Addison-Wesley, Redwood City, 1964).
- [45] B. Schmidt and P. Thalmeier, Anisotropic magnetic and quadrupolar H - T phase diagram of CeRh_2As_2 , *Phys. Rev. B* **110**, 075154 (2024).
- [46] We note that the inclusion of thus far disregarded potential in-plane (E_{g-}) FM magnetic contributions and their couplings to the superconducting OPs could yield an alternative explanation.
- [47] G. Chajewski and D. Kaczorowski, Discovery of Magnetic Phase Transitions in Heavy-Fermion Superconductor CeRh_2As_2 , *Phys. Rev. Lett.* **132**, 076504 (2024).
- [48] A. P. Schnyder and P. M. R. Brydon, Topological surface states in nodal superconductors, *Journal of Physics: Condensed Matter* **27**, 243201 (2015).
- [49] K. Hoshi, R. Kurihara, Y. Goto, M. Tokunaga, and Y. Mizuguchi, Extremely high upper critical field in BiCh_2 -based (Ch: S and Se) layered superconductor $\text{LaO}_{0.5}\text{F}_{0.5}\text{BiS}_{2-x}\text{Se}_x$ ($x = 0.22$ and 0.69), *Sci. Rep.* **12**, 288 (2022).
- [50] P. Miles, S. Kennedy, G. McIntyre, G. Gu, G. Russell, and N. Koshizuka, Refinement of the incommensurate

- structure of high quality Bi-2212 single crystals from a neutron diffraction study, [Physica C: Superconductivity](#) **294**, 275 (1998).
- [51] K. Gotlieb, C.-Y. Lin, M. Serbyn, W. Zhang, C. L. Smallwood, C. Jozwiak, H. Eisaki, Z. Hussain, A. Vishwanath, and A. Lanzara, Revealing hidden spin-momentum locking in a high-temperature cuprate superconductor, [Science](#) **362**, 1271 (2018).
- [52] W. A. Atkinson, Microscopic model for the hidden Rashba effect in $\text{YBa}_2\text{Cu}_3\text{O}_{6+x}$, [Phys. Rev. B](#) **101**, 024513 (2020).
- [53] X. Lu and D. Sénéchal, Spin texture in a bilayer high-temperature cuprate superconductor, [Phys. Rev. B](#) **104**, 024502 (2021).